

Full Length Article

# In-depth analysis of the influence of bio-silica filler (*Didymosphenia geminata* frustules) on the properties of Mg matrix composites

Izabela B. Zgłobicka<sup>a,\*</sup>, Anna Dobkowska<sup>b,c,\*</sup>, Aleksandra Zielińska<sup>b</sup>, Ewa Borucinska<sup>a</sup>,  
Mirosław J. Kruszewski<sup>b</sup>, Rafał Zybala<sup>b,c</sup>, Tomasz Płociński<sup>b</sup>, Joanna Idaszek<sup>b</sup>,  
Jakub Jaroszewicz<sup>b</sup>, Krystian Paradowski<sup>b</sup>, Bogusława Adamczyk-Cieślak<sup>b</sup>,  
Kostiantyn Nikiforow<sup>d</sup>, Bartosz Bucholc<sup>c,e</sup>, Wojciech Świążkowski<sup>b</sup>, Krzysztof J. Kurzydłowski<sup>a</sup>

<sup>a</sup> Faculty of Mechanical Engineering, Białystok University of Technology, Wiejska 45C, 15-351 Białystok, Poland

<sup>b</sup> Faculty of Materials Science and Engineering, Warsaw University of Technology, Woloska 141, 02-507 Warsaw, Poland

<sup>c</sup> Lukaszewicz Research Network – Institute of Microelectronics and Photonics, Al. Lotników 32/46, 02-668 Warsaw, Poland

<sup>d</sup> Institute of Physical Chemistry Polish Academy of Sciences, Kasprzaka 44/52, 01-224 Warsaw, Poland

<sup>e</sup> Institute of Fundamental Technological Research Polish Academy of Sciences, Pawinskiego 5B, 02-106, Warsaw, Poland

Received 21 April 2023; received in revised form 5 July 2023; accepted 10 August 2023

Available online 1 September 2023

## Abstract

A novel metal matrix composites (MMC) with Mg matrix reinforced with natural filler in the form of *Didymosphenia geminata* frustules (algae with distinctive siliceous shells) are presented in this work. Pulse plasma sintering (PPS) was used to manufacture Mg-based composites with 1, 5 and 10 vol.% ceramic filler. As a reference, pure Mg was sintered. The results show that the addition of 1 vol.% *Didymosphenia geminata* frustules to the Mg matrix increases its corrosion resistance by supporting passivation reactions, and do not affect the morphology of L929 fibroblasts. Addition of 5 vol.% the filler does not cause cytotoxic effects, but it supports microgalvanic reactions leading to the greater corrosion rate. Higher content than 5 vol.% the filler causes significant microgalvanic corrosion, as well as increases cytotoxicity due to the greater micro-galvanic effect of the composites containing 10 and 15 vol.% diatoms. The results of contact angle measurements show the hydrophilic character of the investigated materials, with slightly increase in numerical values with addition of amount of ceramic reinforcement. The addition of *Didymosphenia geminata* frustules causes changes in a thermo-elastic properties such as mean apparent value of coefficient of thermal expansion (CTE) and thermal conductivity ( $\lambda$ ). The addition of siliceous reinforcement resulted in a linear decrease of CTE and reduction in thermal conductivity over the entire temperature range. With the increasing addition of *Didymosphenia geminata* frustules, an increase in strength with a decrease in compressive strain is observed. In all composites an increase in microhardness was attained.

The results clearly indicate that filler in the form of *Didymosphenia geminata* frustules may significantly change the most important properties of pure Mg, indicating its wide potential in the application of Mg-based composites with a special focus on biomedical use.

© 2023 Chongqing University. Publishing services provided by Elsevier B.V. on behalf of KeAi Communications Co. Ltd.

This is an open access article under the CC BY-NC-ND license (<http://creativecommons.org/licenses/by-nc-nd/4.0/>)

Peer review under responsibility of Chongqing University

**Keywords:** Metal-matrix composites (MMCs); Pulse plasma sintering (PPS); Ceramic filler; Microstructure; Properties.

## 1. Introduction

The necessity of lightweight materials for use in various applications, i.e., automotive [1,2], aerospace [3], biomed-

cal applications [4], computer, communication and consumer products, has spurred widespread efforts to develop novel metal matrix composites (MMC). Considering the strength-to-weight ratios of metals, Mg has ideal ductility and castability

\* Corresponding authors.

E-mail addresses: [izglobicka@pb.edu.pl](mailto:izglobicka@pb.edu.pl) (I.B. Zgłobicka), [anna.dobkowska@pw.edu.pl](mailto:anna.dobkowska@pw.edu.pl) (A. Dobkowska).

properties because of the lower density ( $1.74 \text{ g/cm}^3$ ), which is two-thirds that of Al, one-fourth of Zn, and one-fifth of steel [5,6]. The good machinability of Mg allows it to be shaped with numerous methods such as powder metallurgy, casting, plastic deformation, and other [7]. Comparison to other metals and polymers shows Mg has better thermal and electrical conductivity, vibration and shock absorption as well as damping capacity [8–10]. It also presents no toxicity hazard [11]. However, the main obstacle to the wide use of Mg and its alloys is their proneness to corrosion. This is a serious problem in clinical use, when the high corrosion rate causes hydrogen release in the surroundings of implants [12,13].

The properties of Mg and alloys can be significantly improved using micro/nano-sized particles. Apart from improving the aforementioned characteristics, the material may be also tailored to a variety of specific applications with the addition of various reinforcements. For example, the addition of ceramic particles into the Mg matrix to improve the ductility, reduce the grain size and weaken the texture of Mg [14–16]. Some of the most commonly used additions are titanium dioxide ( $\text{TiO}_2$ ) [17–19], zirconium oxide (ZrO) [20–25], hydroxyapatite (HAp) [26–29], beta-tricalcium phosphate ( $\beta$ -TCP) [30,31], calcium polyphosphate (CPP) [27], fluorapatite (FAP) [32], bioactive glass (BG) [33–39], bredigite (Bre) [40,41], zinc oxide (ZnO) [42], and magnesium oxide (MgO) [43–45]. Hydroxyapatite (HAp), improves biocompatibility, corrosion and the mechanical resistance [26–29]. Composites of Mg/HAp, varying in composition and grain size, are manufactured *via* spark plasma sintering (SPS) method and demonstrated better mechanical characteristics and corrosion resistance than pure Mg [46]. Investigations of the influence of  $\beta$ -tricalcium phosphate ( $\beta$ -TCP) revealed an increase in hardness values with the increasing content of ceramic reinforcement [30]. According to Cui *et al.* [30], the particles which are harder than the matrix (Mg-Zn-Zr alloy, ZK61), limit at local deformation of the matrix. In comparison to pure ZK61, the composite has higher compressive strength. It is explained by the reduction of the grain size of the ZK61 alloy and that fine grains hinder dislocation movement [30]. Comparing the additions of  $\beta$ -TCP and HAp, the former shows better solubility in human body fluid [26,31]. Composites with the uniformly distributed bioactive glass (BG) demonstrate an increase in corrosion resistance over pure Mg [47]. The mesoporous bio-glass (MBG) created by Yang *et al.* [33] results in *in-situ* apatite layer deposition which reduced the corrosion rate of the Mg matrix. The addition of BG particles also has a positive impact on the micro-hardness of the composites [34]. Among the other reinforcements, BG demonstrates better solvability and biodegradable corrosion products [35–38]. Furthermore, BG forms favorable physical bonds with bone, stimulating bone growth far away from the implant location [37,39]. The increase in mechanical properties as well as a controllable degradation rate was obtained by the addition of calcium polyphosphate (CPP) [27]. Such properties allow us to consider application of Mg-CPP composites as load-bearing bone implants. Results obtained by Lei *et al.*

[42] show that the addition of ZnO to pure Mg results in increases in tensile strength and hardness, as well as in better corrosion resistance.

While the thermal properties of materials containing metallic and ceramic phases are important because of their application at elevated temperature, they have been relatively less studied. The interplay between numerous factors, *i.e.*, significantly different coefficient of thermal expansion (CTE) of metallic and ceramic phases, the effect of processing induced residual stress, initiation of early plastic deformation in the metallic phase, in metal/ceramic composites results in complex behavior of thermal expansion [48]. Each of these factors depend on variety of other parameters. In the case of coefficient of thermal expansion, it is a complex function of temperature which depends on the composition, volume fraction of components and also fabrication process [49]. It must be noted that studies on thermal expansion behavior of metal/ceramic composites were mainly carried out with ceramic reinforcements in form of particles or continuous fibers [50–52]. The differences in the CTE of the matrix and the ceramic reinforcement may result in thermally induced stresses which, when subjected to major temperature cycling, can lead to eventual failure. The mismatch issue of CTE coefficients is also important from the point of view of their applications *i.e.*, in electronics, where components made of different materials interact with each other [53]. Hence, the need for intentional tuning of CTE values can be crucial in order to avoid or reduce the impact of this mismatch.

Another important property determining the potential application of MMC is thermal conductivity ( $\lambda$ ). The ability to dissipate heat efficiently limits possible overheating which could occur when the material is under operational conditions. Therefore, the effective transfer of thermal energy to the environment may become of the highest priority, and thus the highest possible thermal conductivity of the material may be desired [54,55]. The intrinsic qualities of these two groups of materials, *i.e.*, metallic and ceramic, are significant differences in thermal conductivities. Among the important factors affecting composite properties are the size and content of the reinforcing ceramic particles as well as phonon scattering phenomena occurring at the metal matrix-ceramic particle interface [56]. The addition of finely dispersed, small high-strength particles into ductile metal matrix results in the formation of the strengthening mechanisms related to the hindering of the sliding and climbing of dislocations. Concurrently, it is usually accompanied by a deterioration of thermal properties such as conductivity or the aforementioned CTE [57]. Reinforcement in the form of particles with a poor thermal conductivity (such as ceramics) into a highly conductive metallic matrix, may lower the ability to dissipate the heat.

To overcome limitations in ceramic reinforcement availability, for the first time we used a unique bio-based filler in the form of diatom frustules as Mg reinforcement. The siliceous frustules of diatoms, unicellular eukaryotic algae, possess unique species specific, three-dimensional hierarchi-

cal architecture [58]. The properties of diatoms frustules show their affinity as candidates for applications in mechanical, electrical and photonic industrial sectors [59,60]. The specific advantage of frustules is their unique architecture which makes them act as ribbed cavities when added to the composite matrix, leading to the reduction of the specific weight without reducing the strength, which for modern industry is of crucial importance. Recent studies show that reinforcing various matrices, metallic as well as polymeric, with bio-silica diatom frustules allows for new light materials with enhanced mechanical properties to be obtained [61–65]. One example of this is the fabrication of Ti6Al4V-DE composites *via* spark plasma sintering (SPS) shown in previous work by Zgłobicka et al. [64].

The commonly used methods for manufacturing of Mg-based composites are powder metallurgy [66–72], casting [73–75], wrought techniques [76,77] and additive manufacturing [78–82]. Those methods have a direct effect on the microstructure as well as the properties of the composites, *i.e.*, mechanical properties, corrosive and biological behavior [74,83,84]. Among these techniques, powder metallurgy is the most common, and allows the uniform distribution of reinforcement within the matrix at low manufacturing temperature and low-cost [30,38,46]. The entire production process may be described in three steps: blending of the powders, compaction, and sintering. In case of the ceramic filler, the limitations of wettability of ceramic particles with the molten metal matrix may be omitted.

With regard to technological and biomedical concerns, researchers and technologists look for naturally occurring reinforcement which may enhance the properties of Mg-based composite materials. Therefore, here we explore the possibilities of fabrication of Mg-based composited reinforced with diatom frustules obtained from natural sources, using pulse plasma sintering (PPS). To the best of our knowledge, this is the first study, where the properties of Mg-based composites with diatom frustules (*Didymosphenia geminata*) as a ceramic filler, are described. The main goal of this paper is to analyze the microstructural evaluation due to various ceramic filler content in the Mg matrix (1, 5 and 10 vol.% diatom frustules), and subsequent corrosive, biological, thermal, thermo-elastic and mechanical properties changes.

## 2. Composites manufacturing

### 2.1. Precursors preparation

Mg-based composites were manufactured from the high purity Atomised Magnesium Powder Société pour la Fabrication du Magnésium (SFM, UNS 1418 with the particle size of 25–80  $\mu\text{m}$ ) and siliceous diatom frustules of *Didymosphenia geminata* obtained from nature (called wild samples) were used as a composite filler [58,85,86]. The preparation procedure included boiling the wild samples in 37% hydrogen peroxide ( $\text{H}_2\text{O}_2$ ) for 12 h to remove organic matter and rinsing in deionized water. Mixtures of Mg powder and diatom frustules in 1%, 5% and 10% additions (by volume) of *Didymosphenia geminata* were obtained by mixing for 1 hour using Turbulatype mixer (Fig. 1a). Pure Mg was also sintered as a reference material. No balls were used for mixing to provide maximum purity and prevent the fracturing of *Didymosphenia geminata* frustules.

### 2.2. Manufacturing method

The composites were consolidated using pulse plasma sintering (PPS). In PPS, the pulsed electric current generates Joule heating in the graphite punches, die, and consolidated powder. Similar to other current-assisted powder metallurgy techniques, fast heating rate, shorter annealing time, and enhanced diffusion in the electric field may be achieved [87], which is of crucial importance during sintering of natural filler with Mg matrix. As shown in Fig. 1b, the battery capacitors with a total capacity of 300  $\mu\text{F}$  is charging using a DC power supply. The ignition system is responsible for closing the circuit and discharging the capacitors. The maximum duration of a single pulse is *ca.* 600  $\mu\text{s}$ , while the set time between the pulses can range from fractions of a second to less than 10 s. The whole process of consolidation is carried out in a vacuum chamber. The powder mixture is placed in a graphite matrix between two graphite punches, which act as electrodes. The system is heated up *via* periodic current pulses flowing through both the powder and the die. Because of the impulsive character of the energy supply, during the consolidation process there are two temperatures – fixed and instantaneous

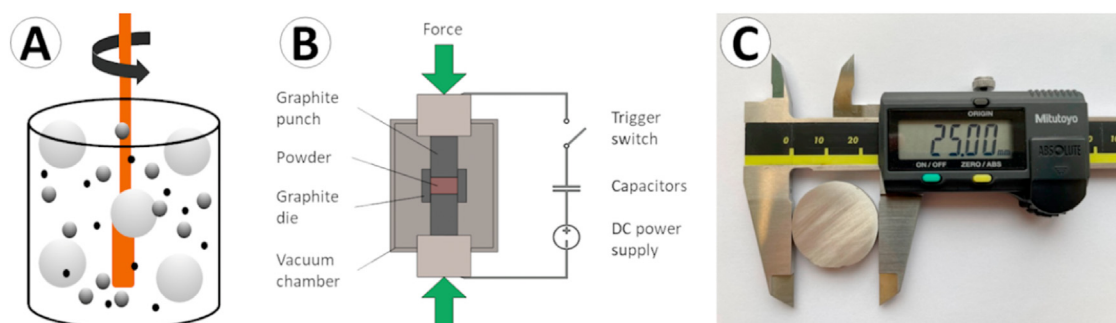


Fig. 1. (A) Scheme of mixture preparation, (B) manufacturing method – pulse plasma sintering, and (C) real life images of the sintered materials.

caused by the flow of a current pulse (higher than the fixed one).

The PPS was conducted under a vacuum. The powder mixtures were placed in a cylindrical graphite die with an inner diameter of 25 mm and pressed between two graphite punches under 19 MPa of initial uniaxial compressive pressure. The mixtures were heated up to 550 °C with a heating rate of 90–100 °C/min, after which a final pressure of 60 MPa was applied. The sintering temperature of 550 °C was maintained for 5 min. As a result, round specimens with the dimension of 25 mm and thickness of 5 mm were produced (Fig. 1c). The experimental density (bulk density) of the composites was obtained by the Archimedes method. The obtained relative density of the samples was estimated at 100% of the theoretical value. The theoretical density was calculated using the rule of mixture.

### 3. Experimental techniques

#### 3.1. Materials characterization

Characterization of Mg powder and *Didymosphenia geminata* frustules was carried out using an ultra-high-resolution analytical dual-beam FIB-SEM tool (Scios2 DualBeam, Thermo Fisher Scientific, Waltham, MA, USA). Powder samples were coated with Au (5 nm layer) using a high-vacuum sputter coater (Gatan, Pleasanton, CA, USA). The particles' distribution of the Mg powder and *Didymosphenia geminata* frustules was performed using a laser particle size analyzer (Fritsch, Idar-Obserstein, Germany) in water suspension. The density of the materials was measured using Archimedes method.

The scanning electron microscopic (SEM) images of the samples were performed using field emission microscope Hitachi SU70. To approach samples were ion milled in an Ar<sup>+</sup> beam (Ion Milling System, Hitachi IM4000). To perform detailed observations of the matrix/filler interface, the lamellas were prepared using focus ion beam (FIB) Hitachi NB5000. To avoid oxidation during sample transportation to other equipment, lamellas were analyzed in scanning transmission electron microscope (STEM) using the same equipment. The cross-section observations were performed in a secondary electron (SE) mode and using atomic mass contrast in transmission mode taken on annular dark field detector (DF). The chemical point analyses using energy dispersive spectrometer (EDS) were made to have a detailed information about chemical constituents formed during material fabrication. The phase compositions of the alloys were determined using X-ray diffraction (XRD, Bruker D8 Advance) operated at 40 kV and 40 mA with Cu-K $\alpha$  radiation. The results were recorded by stepwise scanning  $2\theta$  from 10° to 120°, with a step size of 0.02° and a count time of 10 s per step.

To obtain a detailed description of the microstructure formed during sintering, electron backscattered diffraction (EBSD) was utilized using a scanning electron microscope (SEM, Hitachi SU70) equipped with Bruker EBSD detector. Samples were ion milled in an Ar<sup>+</sup> beam (Ion Milling Sys-

tem, Hitachi IM4000). All EBSD measurements were conducted with a step size of 0.2  $\mu\text{m}$ . The SEM imaging and chemical analyses were conducted using energy dispersive spectrometer (EDS). The crystallographic orientation of grains is presented in the form of inverse pole figures (IPF). Kernel average misorientation (KAM) maps are given to analyze residual stress in the material. The samples were scanned using a micro-focused X-ray tomographic system (MicroXCT-400, Xradia - Zeiss), at 40 kV and 200  $\mu\text{A}$ . For each sample, 1200 projection images were recorded with an exposure time of 5 s and a magnification objective of  $4 \times$ . The volume was reconstructed using the supplied manufacturer software and then exported to Avizo Fire (Thermo Fisher Scientific) for further 3D image analysis. The voxel size was the same for all samples ( $5 \times 5 \times 5 \mu\text{m}$ ).

#### 3.2. Corrosion properties

Corrosion resistance of the materials was characterized based on the electrochemical measurements, while the corrosion rate of composites was determined based on the hydrogen release method. The electrochemical testing was carried out in a phosphate buffered saline (PBS) solution at 37 °C. The PBS was prepared using tablets purchased from Sigma Aldrich Ltd. (1 liter of PBS was prepared using 5 tablets). Open circuit potential ( $E_{\text{OCP}}$ ) during 1 h of immersion, electrochemical impedance spectroscopy (EIS) and potentiodynamic measurements were acquired using a setup composed of Pt wire as a counter electrode, Ag/AgCl as the reference electrode and the Mg sample as a working electrode. After 1 h of immersion, EIS were recorded in a range of 0.01 Hz to 10,000 Hz. Potentiodynamic scans were registered starting from 0.5 V below  $E_{\text{OCP}}$ , finishing at 2 V vs  $E_{\text{OCP}}$ . The EIS and potentiodynamic polarization results were fitted using Gamry Echem Analyst<sup>TM</sup> software. To ensure the reproducibility of the results, at least three measurements for each sample were made. The characterization of the corroded surfaces was performed by SEM (Hitachi SU70) after immersion for 1 h in PBS at 37 °C. Samples were observed covered with corrosion products and after the removal of corrosion products. Corrosion products were removed by chemical treatment with CrO<sub>3</sub> for 40 s as specified in Dobkowska *et al.* [88]. The corrosion rate of the samples was evaluated based on the hydrogen release method. Three samples from each material were polished up to #4000-grit SiC paper, cleaned, and measured. Afterwards, they were placed into the beaker connected to a burette where the hydrogen gas was collected [89,90]. The chemical composition of the corrosion products was analyzed based on X-ray photoelectron spectroscopy (XPS) PHI 5000 VersaProbe (Scanning ESCA Microprobe ULVAC-PHI) with a monochromatic Al K $\alpha$  X-ray source ( $h\nu = 1486.6 \text{ eV}$ ). Survey spectra and high-resolution spectra were recorded using pass energies of 117.4 and 23.5 eV. Peaks were fitted using an asymmetric Gaussian/Lorentzian mixed function using CasaXPS software (version 2.3). The XPS signal intensity was determined using linear or Shirley background subtraction.

### 3.3. Wettability

Contact angle measurements were performed by the sessile drop technique at room temperature and atmospheric pressure, with a Osilla Contact Angle Goniometer (Osilla, Sheffield, UK). Ten independent measurements were performed for each sample, each with a 2  $\mu$ L deionized water drop. In order to examine the macroscopic characteristic and to eliminate the effect of topography, the measurements of contact angle were conducted on the polished cross-sections. The results were then averaged to reduce the impact of surface nonuniformity.

### 3.4. Biological properties

The cytotoxicity of the pristine Mg and its composites was evaluated according to ISO 10993-5 guidelines [91] using the L929 murine fibroblasts cell line (ECACC, Sigma-Aldrich) and human bone marrow-derived mesenchymal stem cells (hMSC, Lonza). The samples were cleaned for 15 min. in acetone and then 15 min. in ethanol, followed by drying in a laminar flow cabinet and exposure to UV light (30 min. for each side). To prepare the extracts, sterile specimens were immersed in 0.42 ml of either Dulbecco's modified eagle medium (DMEM, Gibco, UK, cat. no. 10566016) or Minimum Essential Medium alpha ( $\alpha$ MEM, Gibco, UK, cat. no. 32561037), and incubated at 37 °C and 5% CO<sub>2</sub> atmosphere for 24 h. The medium volume was calculated based on the guidelines for standard surface area and extract liquid volumes; however, it had to be increased by 25% to ensure complete immersion of the samples in the 48-well plates. Media without samples were incubated as a control.

L929 cells were cultured in DMEM supplemented with 10% of fetal bovine serum (FBS, EuroClone, Italy), 1% of penicillin and streptomycin (PS, Gibco, UK) and 2 mM of L-glutamine (Sigma-Aldrich, USA). hMSC were expanded in  $\alpha$ MEM supplemented with 10% of FBS, 1% of PS and 1 nM of fibroblast growth factor 2 (Sigma-Aldrich, Israel). To study the cytotoxicity, the cells were seeded in 96-well plates at densities of either  $10 \times 10^3$  (L929 cell) or  $5 \times 10^3$  (hMSC) and allowed to adhere and spread overnight. On the next day, the DMEM and  $\alpha$ MEM extracts were supplemented with 10% FBS, 1% PS and 2 mM of L-glutamine (DMEM only), added to wells with L929 cells (DMEM extracts) and hMSC ( $\alpha$ MEM extracts), and incubated with the cells for 24 h. To evaluate the effect of soluble corrosion products on viability of the cells, a MTS assay (Promega, USA) was performed according to protocol established by the manufacturer. The absorbance was measured at  $\lambda=490$  nm using Fluorostar Omega plate reader (BMG Labtech). The results were analyzed statistically by means of one-way ANOVA followed by Tukey-Kramer pair-wise comparisons (KyPlot software, version 2.0 beta). The morphology of the cells after incubation with the extracts was visualized by PrimoVert inverted microscope (Zeiss, Germany) at magnification of  $200 \times$  and recorded using Zen 3.6 software.

### 3.5. Thermal and thermo-elastic properties

The coefficient of thermal expansion (CTE) was measured using a DIL 402 Expedit (Netzsch, Selb, Germany) apparatus. The test samples were rectangular cuboids with dimensions of 3 mm  $\times$  3 mm  $\times$  24 mm.

The thermal conductivity,  $\lambda$ , was calculated according to the Eq. (1):

$$\lambda = \rho \cdot C_p \cdot \alpha \quad (1)$$

where  $\rho$  (g/cm<sup>3</sup>) is a density measured with the Archimedes principle,  $C_p$  (J/g·K) is the theoretical heat capacity, and  $\alpha$  (mm<sup>2</sup>/s) is a thermal diffusivity measured with a laser flash method (LFA) by the means of LFA 457 MicroFlash equipment (Netzsch, Selb, Germany). To determine  $\lambda$  of the composites, the specific heat value was assumed to be 1.02 J/g·K for pure Mg according to Lee *et al.* [9]. Samples for thermal diffusivity measurements were cylinders with a diameter of 10 mm and height of 1 mm.

Both  $\alpha$  and CTE measurements were performed over a temperature range from 50 to 400 °C in the inert atmosphere of Ar.

### 3.6. Mechanical properties

Mechanical properties were tested using compression tests at room temperature. The specimens had the cylindrical form with a length to diameter ratio of 3:2 (3 mm of length to 2 mm of diameter). The measurement of the loading force was carried out using a force sensor with an accuracy of  $\pm 2$  N. The deformation of the samples with the rate of 0.5 mm/min was carried out by moving the traverse of the Zwick/Roell testing machine. The criterion for stopping the test was a 30% drop in compressive force from the maximum value. The stress value was calculated using the initial cross-section of the samples. During analysis, the values of compressive yield strength ( $\sigma_{YS}$ ) and compressive strength ( $\sigma$ ) were determined. The offset for calculation  $\sigma_{YS}$  had value 0.2% of compressive strain. Tests were repeated for 3 samples from each material. The representative light microscopy images of the samples before and after mechanical tests were documented.

The microhardness of the composites was tested by the Vickers method using a Hardness Tester InnovaTest Falcon 500 under the load HV0.2. Ten measurements in line were made for each sample with a distance of 0.35 mm between the subsequent indentations.

## 4. Results

### 4.1. Precursors characterization

Shape, size and morphology of the Mg powders and frustules of *Didymosphenia geminata* were observed using SEM (Fig. 2). Mg particles are spherical with no visible porosity (Fig. 2a-b). Some of bigger particles, with diameter larger than 30  $\mu$ m, have satellites attached onto their surface

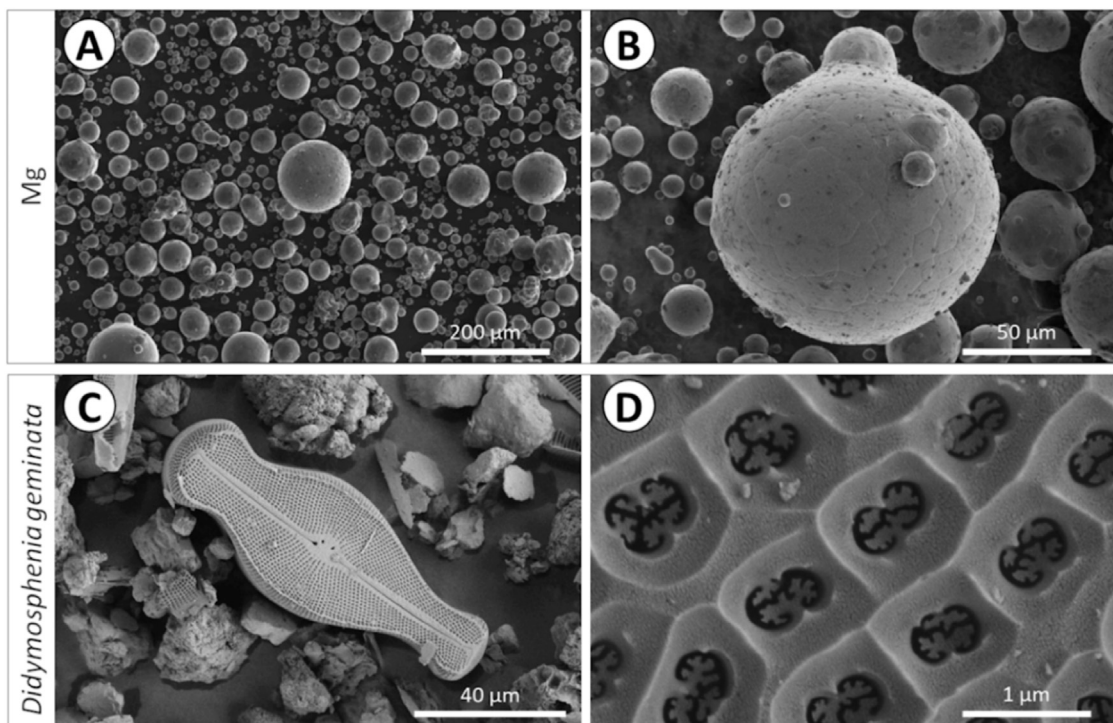


Fig. 2. SEM morphologies of (A-B) as-received Mg particles and (C-D) as prepared *Didymosphenia geminata* frustules.

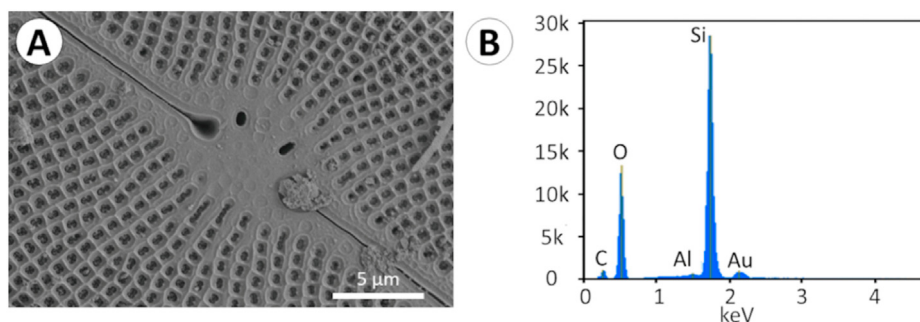


Fig. 3. (A) SEM morphology and (B) EDS analysis of the as prepared *Didymosphenia geminata* frustules.

(Fig. 2b). In the mixtures prior to sintering, whole as well as fragmented frustules may be distinguished (Fig. 2c). The characteristic feature of the main diatom taxon, *Didymosphenia geminata*, is its morphology, see Fig. 2d. This morphology is of a biraphid pennate diatom with capitate ends and an inflated center. Openings across the frustule, called areolae, have a funnel shape.

The average diameter of Mg powder  $45.6 \pm 0.7 \mu\text{m}$  determined by the laser particle size analyzer, is in agreement with the manufacturer's data. The size of the particular frustule is in the range of 120–140  $\mu\text{m}$  in length and 35–45  $\mu\text{m}$  in width. The chemical elemental analysis of *Didymosphenia geminata* frustules shown in Fig. 3b confirms the presence of Si and O. The presence of C, Au and Al are artefacts resulting from the sample preparation procedure (coating with Au) and Al stub with C tape.

## 4.2. Composites

### 4.2.1. Microstructural description

The microstructures of the sintered materials are depicted in Fig. 4 and Fig. 5. Clearly distinguishable multi-grained Mg particles with dark contrast areas located at the particle boundaries are visible on the SEM image (Fig. 4a). The microstructures of the Mg with the addition of ceramic filler are shown in Fig. 4b-d. As observed, siliceous frustules built themselves into interparticle spaces (Fig. 4b-d, yellow arrowheads).

One feature characteristic of the diatom frustules, ribs, are well distinguishable and easy to identify in SEM images (Fig. 4b-d).

The red arrowheads show the dark contrast areas which exist in both, pure Mg and Mg composites (inset B1 in Fig. 4b). We suppose those may be identified with a mix-

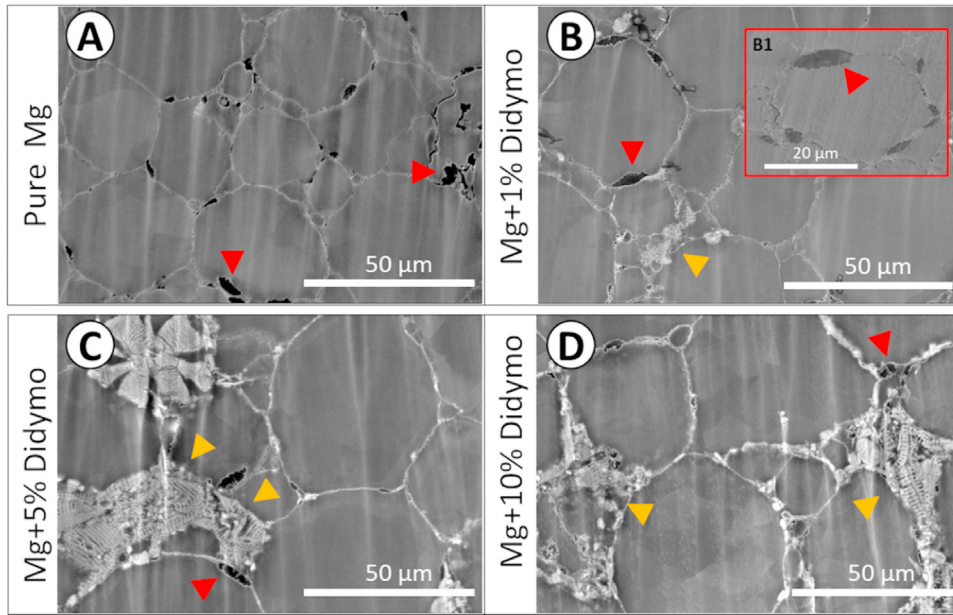


Fig. 4. SEM images of the composites: (A) pure Mg, (B) Mg + 1% *Didymosphenia geminata* frustules, (C) Mg + 5% *Didymosphenia geminata* frustules, (D) Mg + 10% *Didymosphenia geminata* frustules; *Didymosphenia geminata* frustules - yellow arrowheads, MgO/Mg(OH)<sub>2</sub> - red arrowheads.

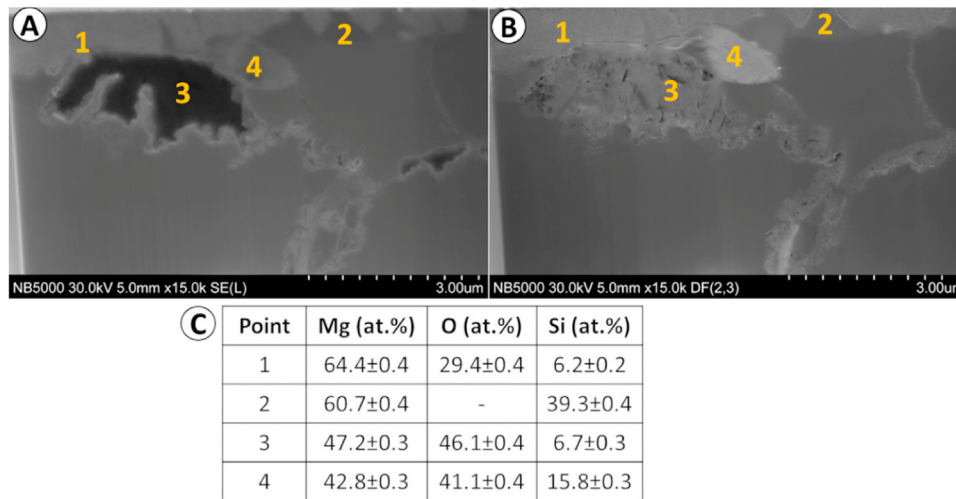


Fig. 5. The representative cross sectional STEM images performed for the Mg + 1% *Didymosphenia geminata* frustules in secondary electron (SE) mode (A) and in dark field (DF) mode (B). Chemical point analyses are shown in panel (C).

ture of MgO/Mg(OH)<sub>2</sub> formed in situ during sintering [42]. To describe the interface between filler and Mg matrix, the cross sectional observation were performed on the lamella prepared from the Mg + 1% *Didymosphenia geminata* frustules (Fig. 5). The same area of interest shown in both, secondary electron (SE, Fig. 5a) and dark field (DF, Fig. 5b) modes, allows to state that the interface between filler and a matrix is continuous, without any segregation and impurities observed. To identify compounds formed during sintering, the chemical analyses on the cross section in points 1–4 were performed. Based on the combined results of chemical and phase analyses (Fig. 5c and 6) it is reasonable to deduce that during sintering Mg<sub>2</sub>Si itself and the mixtures of Mg-Si-O were formed. The atomic ratio of Mg to Si

about 2:1 was found in point 2 indicating presence of Mg<sub>2</sub>Si, while points 1, 3 and 4 are most likely mixtures of MgO and Mg<sub>2</sub>Si. It can be thus concluded that PPS used here induced reactive bonding between silica in frustules and Mg powder.

Porosity and distribution of the diatom frustules were investigated via the  $\mu$ CT method. The 3D reconstructions of the samples' structures revealed that during PPS the fractions of the *Didymosphenia geminata* fillers remain nearly at the same level as theoretical, and as shown in Fig. 7a-c, the calculated volume of ceramic filler is 0.95% for Mg with the addition of 1 vol.% ceramic filler, 4.56% for the sample with the addition of 5 vol.% the filler, and 7.85% for the samples with the addition of 10 vol.% the filler. The images reveal

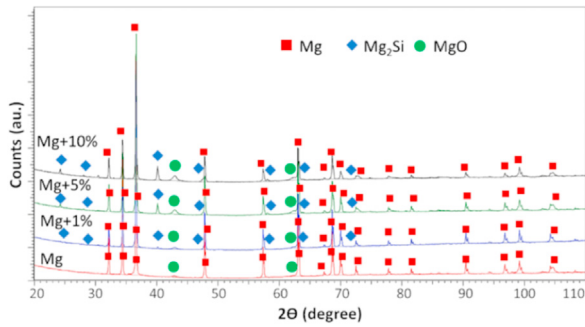


Fig. 6. XRD patterns obtained for the investigated composites.

Table 1

Experimental density of the manufactured materials.

Materials	$\rho_{\text{exp}}$ ( $\text{g} \times \text{cm}^{-3}$ )
Pure Mg	1.75
Mg+1% <i>Didymosphenia geminata</i>	1.76
Mg+5% <i>Didymosphenia geminata</i>	1.89
Mg+10% <i>Didymosphenia geminata</i>	1.83

that frustules are well dispersed and their spatial distribution within Mg matrix is uniform. We observed minimal porosity through the sintered samples, and this is in agreement with the experimental density confirming that consolidation parameters were chosen properly (Table 1). With the increasing concentration of ceramic filler, the porosity of the materials also rises (Fig. 7d-g), in non-linear increase. The lowest porosity was found to be in pure Mg and Mg with the addition of 1 vol.% the *Didymosphenia geminata* frustules. It was calculated to be 0.025% for Mg with the addition of 5 vol.% *Didymosphenia geminata*, and 0.134% when 10 vol.% filler was added into Mg. The increasing porosity is related to the structure of the fillers; pores were observed mainly in the interspatial areas of

the ribs in *Didymosphenia geminata* frustules. The explanation of such results may be related to the geometry of single frustule (see Fig. 2c and d), which should be considered as a ‘caged pore’ because of the emptiness inside. The EBSD results show that all materials have random crystallographic orientation (Fig. 8a-d). High angle boundaries (HAGBs) were observed between grains within a single particle. The mapping of specific phases (Mg and Si) shown in Fig. 8e-h confirms that areas visible between particles are identified with *Didymosphenia geminata* frustules. No strain localization was observed inside the grains of Mg with the exception of areas next to the grain boundaries (Fig. 8i-l).

#### 4.2.2. Corrosion properties

The results delivered from the electrochemical measurements in PBS solution are depicted in Fig. 9. With the highest *Didymosphenia geminata* volume in the composites, the increasing trend of open circuit potential ( $E_{\text{OCP}}$ ) is observed (Fig. 9a).

It is important to note that the initial rise in  $E_{\text{OCP}}$  to more positive values is observed for pure Mg, Mg + 1% and Mg + 5% *Didymosphenia geminata*, which after a few minutes of immersion becomes stable. The average value of  $E_{\text{OCP}}$  for pure Mg is the lowest among the investigated alloys, fluctuating around  $-1.65$  V/Ref. A slightly higher  $E_{\text{OCP}}$  is observed for the samples with 1 vol.% filler. Significantly higher  $E_{\text{OCP}}$  is recorded for Mg + 5% *Didymosphenia geminata* ( $-1.55$  V/Ref), while Mg + 10% *Didymosphenia geminata* has the highest values of  $E_{\text{OCP}}$  oscillating around  $-1.52$  V/Ref. From inspection of the measured polarization response of the sample it is possible to deduce that pure Mg, Mg + 5% and Mg + 10% *Didymosphenia geminata* undergo active dissolution in the analyzed solution, while characteristic inflection point ( $E_b$ ) is observed at the anodic branch of the

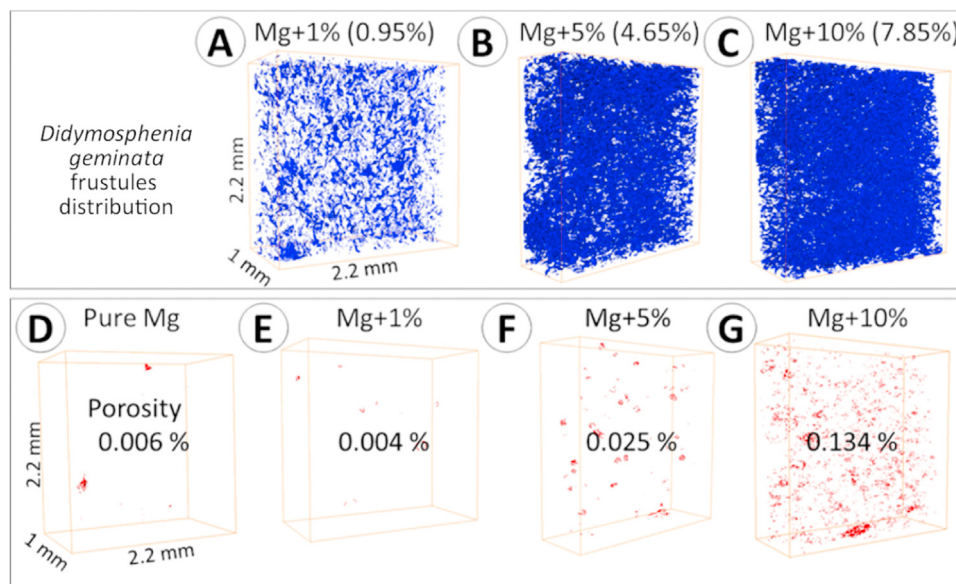


Fig. 7. 3D images showing the diatoms’ frustules distribution (A-C) along with porosity measurements given in vol.% (D-G) obtained from  $\mu$ CT measurements. The calculated from the images volume of the *Didymosphenia geminata* is given in the brackets in panels (A-C).

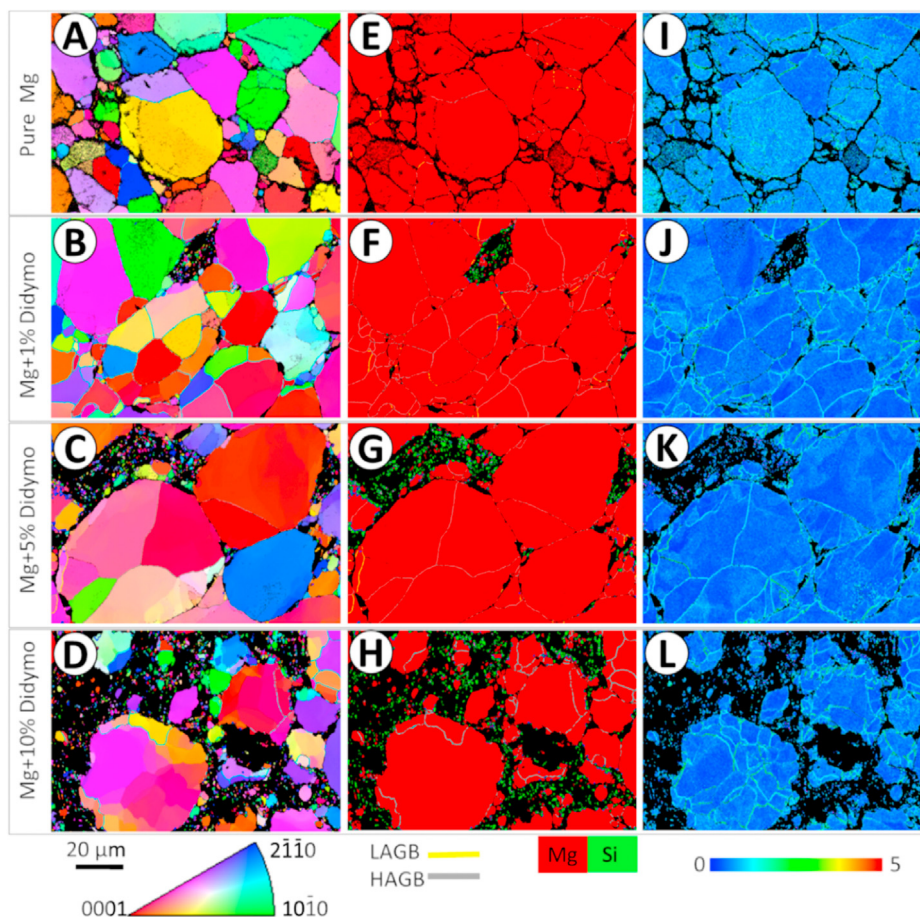


Fig. 8. EBSD data presented in the form of: IPF maps (A–D) with corresponding phase distribution (E–H) and Kernel misorientation maps (I–L). The nonindexed areas are given in black.

Table 2

Characteristic parameters extrapolated from the potentiodynamic measurements shown in Fig. 9b ( $E_{\text{corr}}$  – corrosion potential,  $E_b$  – breakdown potential,  $i_{\text{corr}}$  – corrosion current density, CR – corrosion rate) and  $CR_{\text{HR}}$  calculated based on hydrogen release method.

Material	$E_{\text{corr}}$ (V/Ref)	$E_b$ (V/Ref)	$i_{\text{corr}}$ ( $\mu\text{A}/\text{cm}^2$ )	CR (mpy)	$CR_{\text{HR}}$ (mpy)
Pure Mg	–1.41	n/a	131	293	$1.04 \pm 0.02$
Mg+1% <i>Didymosphenia geminata</i>	–1.40	–1.26	71	160	$1.05 \pm 0.01$
Mg+5% <i>Didymosphenia geminata</i>	–1.38	n/a	251	564	$0.31 \pm 0.02$
Mg+10% <i>Didymosphenia geminata</i>	–1.35	n/a	301	675	$0.38 \pm 0.02$

polarization curve recorded for Mg + 1% of filler (Fig. 9b and Table 3). This inflection point is related to the breakdown of the protective oxide film formed on the composite [92]. Also, the corrosion current density ( $i_{\text{corr}}$ ) is the lowest for this sample (Table 2), indicating that this material is the most resistive in the analyzed solution.

An equivalent electronic circuit (Fig. 9d) is proposed to fit the EIS data.  $R_s$  stands for solution resistance,  $R_a$  and constant phase element ( $\text{CPE}_a$ ) is a resistance and capacitance for electrochemical reactions at the film/Mg interface [93,94].  $R_f$  and  $\text{CPE}_f$  represent the surface film resistance and capacitance. To compensate for the non-homogeneity in the system, a CPE was introduced instead of the capacitor [88,93]. The increasing radius at high and medium frequency capacitive loops clearly indicate that the least reactive in the PBS solu-

tion is the sample with 1% addition of *Didymosphenia geminata*. The corrosion resistance of pure Mg and Mg + 5% *Didymosphenia geminata* is lower, and comparable to each other ( $R_a + R_f$  is relatively similar for both alloys, Table 3). The most active in the analyzed solution is the Mg + 10% of filler. Similar values of  $R_s$  between the reference electrode and the surface of the film-covered Mg electrode indicate that it is not influenced by evolved hydrogen. The increase in  $R_f$  for the Mg with 1% of *Didymosphenia geminata* addition suggests that a significantly less porous film formed on the surface when compared to pure Mg. Simultaneously, lower values of  $R_f$  indicates a higher porosity of the films formed on the Mg with 5 vol.% and 10 vol.% addition of *Didymosphenia geminata*. The results of the electrochemical measurements are in agreement with the corrosion rate calculated

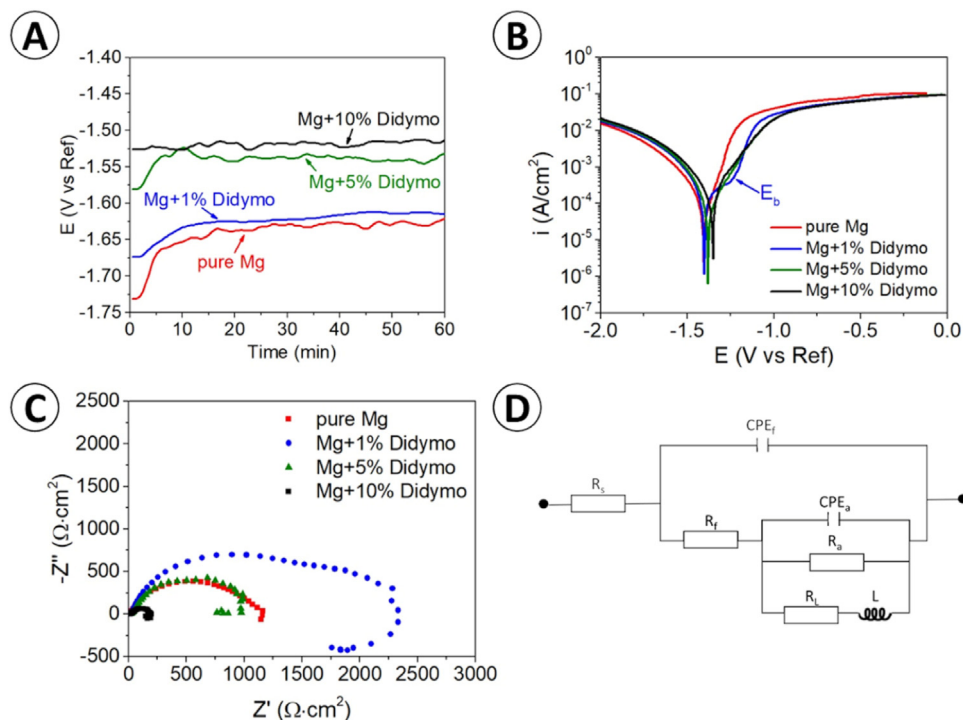


Fig. 9. Results delivered from the electrochemical testing in phosphate buffered saline solution (A) open circuit potential, (B) potentiodynamic curves, (C) Nyquist plots, (D) equivalent electronic circuit used for data fitting.

Table 3

EIS parameters fitted for data shown in Fig. 9c with the EEC given in Fig. 9d.

Material	$R_s$ ( $\Omega \times \text{cm}^2$ )	$R_a$ ( $\Omega \times \text{cm}^2$ )	$\text{CPE}_a$ ( $\mu\text{Ss}^a \times \text{cm}^{-2}$ )	$a_a$	$R_f$ ( $\Omega \times \text{cm}^2$ )	$\text{CPE}_f$ ( $\mu\text{Ss}^a \times \text{cm}^{-2}$ )	$a_f$	$R_L$ ( $\Omega \times \text{cm}^2$ )	$L$ ( $H \times \text{cm}^2$ )
Pure Mg	14	289	154	0.29	878	90	0.74	25	921
Mg + 1% <i>Didymosphenia geminata</i>	17	890	677	0.77	1530	43	0.87	120	6408
Mg + 5% <i>Didymosphenia geminata</i>	22	820	71	0.48	336	46	0.84	298	700
Mg + 10% <i>Didymosphenia geminata</i>	17	132	39	0.91	36	37	0.82	49	4125

using hydrogen evolution method. As shown in Table 2, the comparable corrosion rate is observed for pure Mg and Mg with the addition of 1 vol.% ceramic filler ( $1.04 \pm 0.01$  and  $1.05 \pm 0.02$  mpy, respectively). Higher vol.% *Didymosphenia geminata* resulted in significant corrosion rate increase having  $0.31 \pm 0.02$  and  $0.38 \pm 0.02$  mpy. There is no linear regression line between the points.

The surfaces of the samples after 1 h of immersion in PBS solution is depicted in Fig. 10a-d. A relatively uniform oxide film was formed on pure Mg, with thicker areas located at the particle boundaries (Fig. 10a). Similar corrosion products morphologies were observed on the Mg with the addition of *Didymosphenia geminata* frustules (Fig. 10b-d). As identified by XRD, the main corrosion product formed was MgO (Fig. 10e). The resulting films were characterized by X-ray photoelectron spectroscopy (XPS), which showed the presence of Mg 2p, Na 1s, O 1s, C 1s, P 2p and Si 2p (Table 4). In all cases the Mg 2p peak was fitted at  $\sim 50.7 \pm 0.1$  eV, indicative of Mg–O, in agreement with XRD data. The peak at  $\sim 133.5 \pm 0.1$  eV which corresponds to P2p<sub>3/2</sub> signal was attributed to phosphate groups. The C 1 s spectrum mainly cor-

responds to the so-called adventitious carbon, which is generally composed of various hydrocarbons species with a small amounts of both singly and doubly bound oxygen functionality on the top of all specimen surfaces [95]. Since Si was detected on all samples, we assumed it was built into the surface during samples' polishing resulting in the formation of chemical bonds between silicon and oxygen. In summary, phosphates and magnesium oxides are mainly formed on the surface of the samples.

When the corrosion products were removed, various corrosion mechanisms were clearly distinguishable on the surface of the samples. Examination of the corroded surfaces show that localized corrosion occurred mostly at the particle boundaries (Fig. 11, marked by the red arrowheads). Regardless of the concentration of *Didymosphenia geminata* frustules, those areas were more prone to corrosion due to the pores and the fact that oxides were present at the particle boundaries. Considering pure Mg, some of the deeper localized damage is also visible in the particle's interiors (Fig. 11a, yellow arrowheads). Most importantly, we observed visible corrosion damage inside the particles also formed on the other alloys

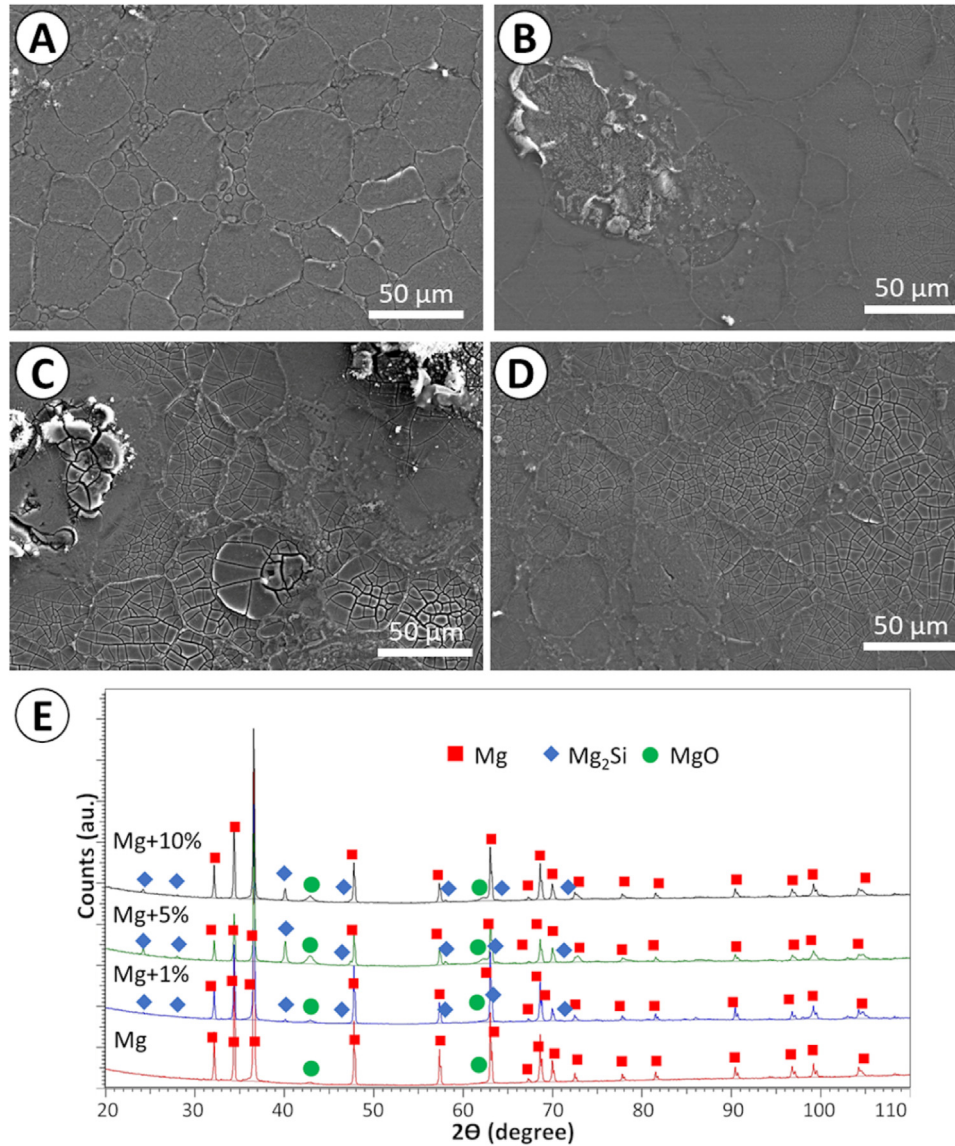


Fig. 10. Characterization of the surfaces after 1 h immersion in PBS at 37 °C: surfaces covered with corrosion products: (A) pure Mg, (B) Mg + 1% *Didymosphenia geminata* frustules, (C) Mg + 5% *Didymosphenia geminata* frustules, (D) Mg + 10% *Didymosphenia geminata* frustules, (E) XRD patterns of the corrosion products formed after 1 h immersion in PBS at 37 °C.

Table 4

The binding energy (BE) and atomic% (At.%) of elements formed on the investigated materials after 1 h of immersion in PBS.

Name	Pure Mg		Mg + 1% <i>Didymosphenia geminata</i>		Mg + 5% <i>Didymosphenia geminata</i>		Mg + 10% <i>Didymosphenia geminata</i>	
	BE / eV	At.%	BE / eV	At.%	BE / eV	At.%	BE / eV	At.%
Mg 2p	50.8	14.7	50.7	16.9	50.6	16.0	50.8	19.1
K 2p 3/2			293.1	1.2	293.3	2.3	293.2	0.3
K 2p 1/2			295.9	0.6	296.1	1.2	296.1	0.2
Na 1s	1072.0	1.1	1071.7	4.9	1071.8	6.7	1071.9	2.5
O 1s	531.6	32.2	531.1	25.7	531.2	26.4	531.5	31.0
O 1s	532.9	4.6	532.0	15.8	532.1	16.0	532.4	10.5
O 1s			533.3	4.1	533.3	3.4	534.1	0.9
C 1s	284.7	30.0	284.8	14.6	284.8	10.1	284.8	21.0
C 1s	286.2	3.9	286.0	2.1	285.8	4.1	286.0	2.0
C 1s	288.3	1.5	289.2	0.6	289.7	0.4	289.8	1.5
C 1s	290.0	0.9						
P 2p 3/2	133.6	6.0	133.4	8.6	133.4	8.8	133.6	7.1
P 2p 1/2	134.4	3.0	134.2	4.3	134.2	4.4	134.4	3.5
Si 2p	102.3	2.1	101.8	0.6	101.6	0.3	101.7	0.4

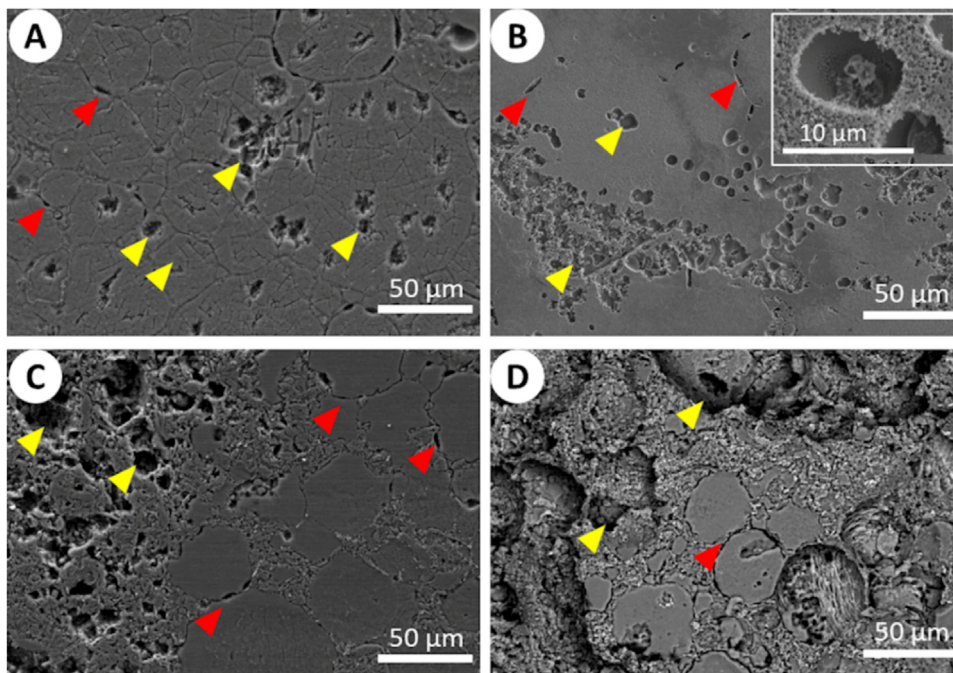


Fig. 11. Characterization of the surfaces after 1 h immersion in PBS at 37 °C: after removal of corrosion products (A) pure Mg, (B) Mg + 1% *Didymosphenia geminata* frustules, (C) Mg + 5% *Didymosphenia geminata* frustules, (D) Mg + 10% *Didymosphenia geminata* frustules.

(Fig. 11b-d). The morphology and the intensity of the dissolved areas change with the increasing concentration of the ceramic filler. In the case of 1 vol.% addition of the ceramic filler, the corroded areas within the particle interiors are not so deep as in the case of pure Mg and were mainly formed in the close vicinity of the ceramic filler (Fig. 11b, yellow arrowheads). More intense damage propagating into the depth of the material is observed in Fig. 11c, where the addition of *Didymosphenia geminata* frustules is 5 vol.%. The maximum intensity of corrosion is visible in Fig. 11d where almost the entire surface of the sample is corroded.

#### 4.2.3. Wettability

The qualitative evaluation of contact angle demonstrates a surface's tendency to repel water. The investigations were conducted with deionized water. The results presented in Table 5 clearly show that addition of 1 vol.% *Didymosphenia geminata* decreased the wettability of surface in comparison to pure Mg, making it the most hydrophobic among all tested materials. Contrary relationship was obtained when the content of *Didymosphenia geminata* frustules was increased to 10 vol.%; the addition of such high vol.% ceramic filler caused the decrease in the numerical values of contact angle, making this material the most hydrophilic.

Table 5  
Results of contact angle measurements using deionized water.

Series	deionized water
Pure Mg	79.5 ± 2.0
Mg+1% <i>Didymosphenia geminata</i>	87.8 ± 4.3
Mg+5% <i>Didymosphenia geminata</i>	83.1 ± 1.7
Mg+10% <i>Didymosphenia geminata</i>	69.6 ± 2.2

#### 4.2.4. Biological properties

Per our results, the samples made of pristine Mg disintegrated completely during first 24 h of incubation in both types of media. All specimens made from Mg with 10 vol.% filler and one specimen prepared from bulk Mg with 5 vol.% *Didymosphenia geminata* started disintegrating in  $\alpha$ MEM medium during first 24 h of incubation. The faster corrosion in the  $\alpha$ MEM could be due to slightly different composition and osmolality of the media ( $\alpha$ MEM: 208–320 mOsm  $\times$  kg<sup>-1</sup>; DMEM: 320–355 mOsm  $\times$  kg<sup>-1</sup>).

The stability of the tested materials was reflected in both cell morphology and viability. DMEM-based extracts of Mg + 1% and Mg + 5% of *Didymosphenia geminata* did not affect the morphology of L929 fibroblasts (Fig. 12a), however, fewer cells could be observed in wells with those extracts, which suggests slight cytotoxicity. Cell density was lower in the case of Mg extracts and Mg + 10% *Didymosphenia geminata*; moreover, the L929 fibroblasts started detaching or seemed to be enlarged. The microscopic observations were confirmed quantitatively by means of a MTS assay, which indicated that the viability of L929 cells was significantly lower than in the control for all test extracts. Furthermore, the drop in cell viability of cells incubated with Mg and Mg + 10% *Didymosphenia geminata* extracts was below 70% (Fig. 12c), indicating cytotoxicity. Viability of L929 cells cultured in media based on extracts Mg + 1% *Didymosphenia geminata* and Mg + 5% *Didymosphenia geminata* reached 76 ± 9% and 78 ± 4% of control, respectively; however, the difference was not significant from the 70% cytotoxicity threshold. Morphology of hMSC cultured with extracts Mg + 1% *Didymosphenia geminata*, and extracts of intact Mg + 5% *Didymosphenia geminata* specimens did not differ from that of the

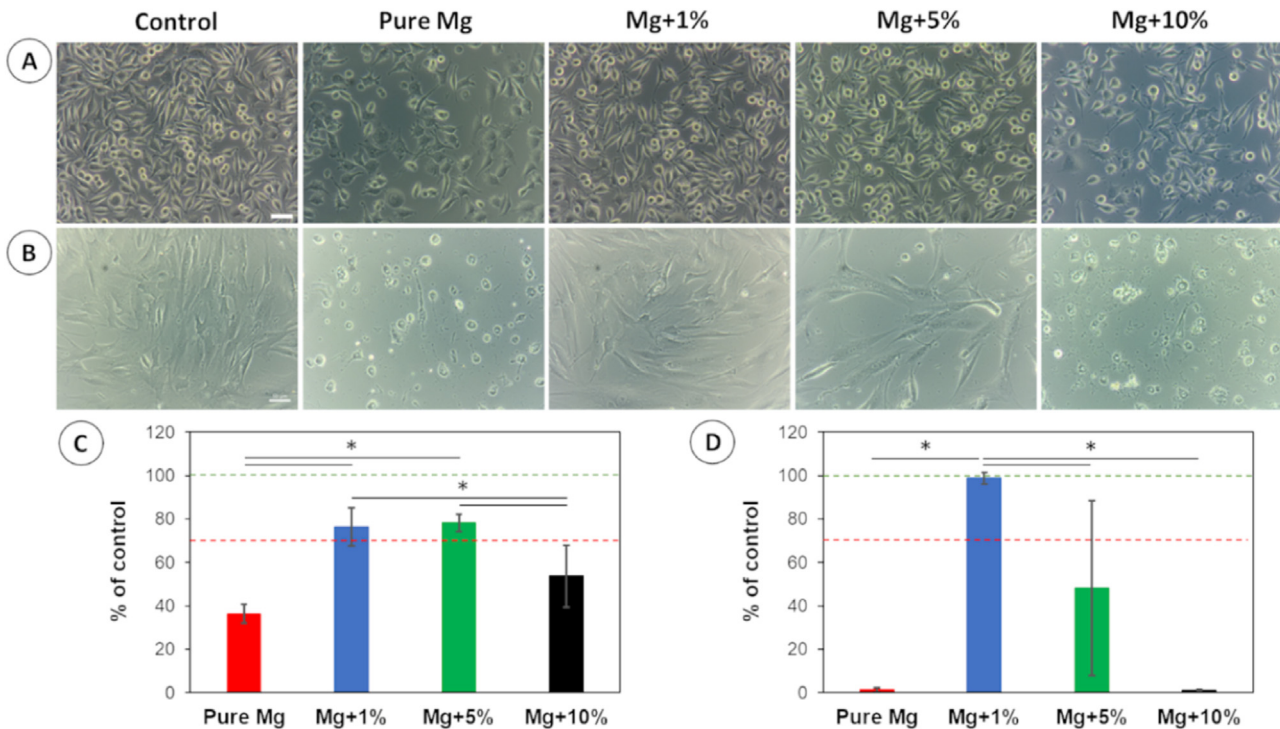


Fig. 12. Evaluation of cytotoxicity. Morphology of L929 (A) and hMSC (B) cells cultured in extracts-based media for 24 h. Scale bar 50  $\mu\text{m}$ . Quantitative assessment of viability of L929 (C) and hMSC (D) cells determined by means of the MTS assay; red dashed line depicts cytotoxicity threshold, while green dashed line depicts the viability of cells cultured in control extracts. \* -  $p < 0.05$ .

Table 6

The coefficient of the thermal expansion (CTE) of the sintered pure Mg and Mg with a ceramic reinforcement.

Series	CTE ( $\text{K}^{-1} \times 10^{-6}$ )
Pure Mg	$29.3 \pm 0.5$
Mg+1% <i>Didymosphenia geminata</i>	$28.8 \pm 0.5$
Mg+5% <i>Didymosphenia geminata</i>	$27.4 \pm 0.4$
Mg+10% <i>Didymosphenia geminata</i>	$25.0 \pm 0.4$

control (Fig. 12b). In contrast, round cells and debris of lysed cells were found in wells containing extract of pristine Mg, Mg + 10% *Didymosphenia geminata* and the disintegrated specimen Mg + 5% *Didymosphenia geminata*. This was confirmed by the MTS assay (Fig. 12d). Therefore, the soluble corrosion products released from the Mg and Mg + 10% *Didymosphenia geminata* materials proved to be extremely cytotoxic for hMSC. The only non-cytotoxic material investigated in this study was Mg + 1% *Didymosphenia geminata* (no significant difference with control).

#### 4.2.5. Thermal and thermo-elastic properties

The manufactured samples were investigated with respect to the coefficient of thermal expansion (CTE) and thermal conductivity ( $\lambda$ ). The results are presented in the Table 6 and Fig. 13, respectively. These two parameters describe thermal behavior of the material in a certain temperature range. The CTE values of the investigated materials, presented in the Table 6, show a linear correlation with the vol.% the rein-

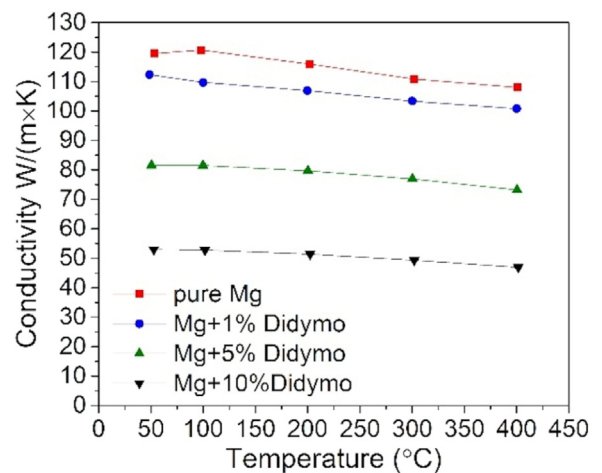


Fig. 13. Thermal conductivity ( $\lambda$ ) of the investigated materials.

forcing phase. As the amount of the natural ceramic addition increased, a decrease in CTE was observed. The addition of 10 vol.% resulted in a 15% reduction relative to the pure Mg. The graphic depiction of the thermal conductivity shows that the decrease in the conductivity for manufactured composite samples is more flattened (ca. 10% of the basic value), Fig. 13. In general, the higher content of the ceramic filler, the lower the thermal conductivity. It was observed that 1, 5 and 10 vol.% addition of *Didymosphenia geminata* resulted in the decrease in thermal conductivity, relative to pure Mg, by 7%, 32% and 65%, respectively.

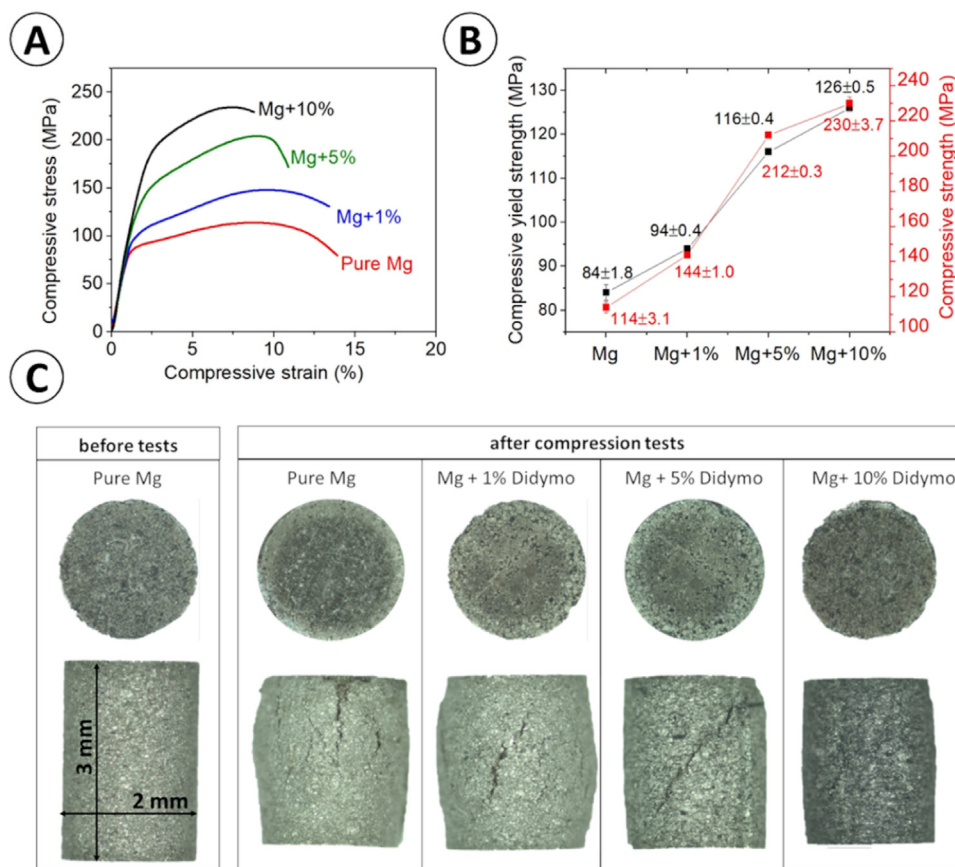


Fig. 14. Results delivered from compression tests: (A) the representative stress-strain curves, (B) calculated values of compressive strength ( $\sigma$ ) and compressive yield strength ( $\sigma_{YS}$ ), (C) light microscopy images of the specimens before and after compression tests.

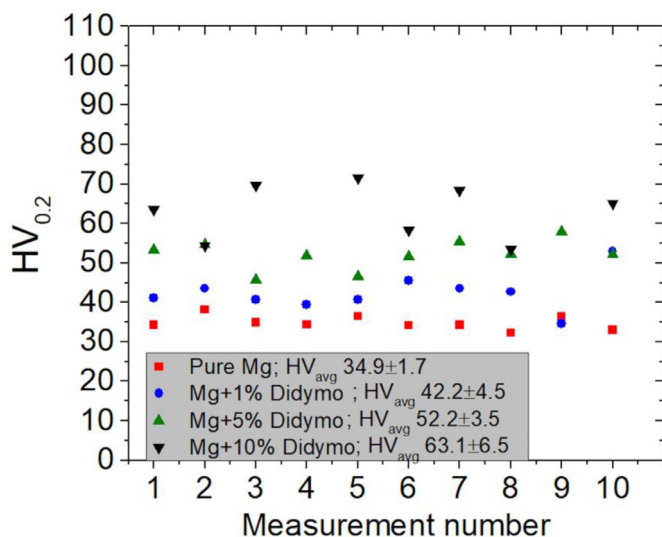


Fig. 15. Microhardness of the investigated samples.

#### 4.2.6. Mechanical properties

The results of the mechanical tests indicate that addition of *Didymosphenia geminata* frustules have positive impact on the compressive stress of the samples (Fig. 14a). With the increased addition of *Didymosphenia geminata* frustules, an

increase in strength with a decrease in compressive strain is observed. The smallest average value of compressive yield strength of 84 MPa was determined for pure Mg, while the addition of *Didymosphenia geminata* frustules increased its values to 94, 116 and 127 MPa for 1, 5 and 10 vol.% *Didymosphenia geminata*, respectively (Fig. 14b). The values of compressive strength also increased with the increasing volume of *Didymosphenia geminata* frustules, from 114 MPa for pure Mg to 144, 213 and 230 MPa for 1, 5 and 10 vol.% *Didymosphenia geminata* addition, respectively (Fig. 14b). The samples after the tests are illustrated in Fig. 14c. As observed, a higher number of cracks are visible on the pure Mg and sample containing 1 vol.% *Didymosphenia geminata* frustules compared to those with 5 and 10 vol.% frustules. The results obtained from the compression tests scales with microhardness values. The addition of diatom frustules results in an increase of the microhardness from 34.9 HV up to 42.5 HV, 52.2 HV and 63.1 HV for 1, 5 and 10 vol.% *Didymosphenia geminata*, respectively (Fig. 15). All values are statistically significant.

## 5. Discussion

In this work, we investigated novel Mg based MMCs with natural ceramic filler in terms of microstructure, corrosion,

biological, thermal, and mechanical properties. Three various concentrations of *Didymosphenia geminata* frustules (1, 5 and 10% by vol.) were added into pure Mg powder and PPSed. As the reference material pure Mg was sintered. The bulk materials were characterized in terms of microstructure, porosity and phase composition. As observed, the distribution of *Didymosphenia geminata* frustules was uniform in all investigated materials, regardless the concentration of the ceramic filler. The addition of 1 vol.% the ceramic filler slightly reduces the porosity of the material when compared to bare Mg. When analyzing 5 and 10 vol.% the ceramic filler, the higher the concentration of the filler, the greater the porosity of the composite. The increasing porosity is related to the structure of the fillers; pores were observed mainly in the interspatial areas of ribs in *Didymosphenia geminata* frustules. The Mg<sub>2</sub>Si, MgO, and their mixtures were detected in the phase composition of the materials investigated in this work, and this can be a result of the following reactions (Eq. (2) and Eq. (3)) [96]:



The formation of the intermetallic phases of Mg<sub>2</sub>Si and MgO in the materials processed by powder metallurgy methods have been already reported [97–99] even at the temperature below 550 °C which was used in this study to sinter MMCs. The intermediate compounds formed in the matrix are well adhesive and the interface between them and the Mg matrix is continuous.

Recently, attention has been paid to the use of powder metallurgy methods to obtain Mg based MMCs with a relatively homogenous distribution of the reinforcement, which may result in the improvement of mechanical properties [96]. None of those works, however, show an apparent positive influence of the reinforcement addition on the corrosive behavior of Mg based MMCs. The addition of SiO<sub>2</sub> to a Mg matrix intensified intergranular corrosion [96]. Tiwari *et al.* [100] investigated SiC reinforced Mg-based MMCs, and found the presence of SiC particles deteriorated the corrosion resistance of Mg. Carbon nanotubes increased mechanical properties, but their presence accelerated corrosion of the matrix [101]. The results of our research clearly define that the trace addition of the ceramic filler and its proper distribution in the Mg matrix may result in improvement in both corrosion and mechanical properties; however, it is related to the restricted concentration of ceramic filler in the Mg matrix. As per results of this work, 1 vol.% the *Didymosphenia geminata* frustules had a positive influence on the corrosion resistance of the Mg sintered *via* PPS. This is related to the decreasing porosity at the particle-particle interfaces where the frustules were built into the metallic matrix during synthesis. Corrosion processes in the case of pure Mg were the most intensified in the areas where the pores were present; however, this mechanism was diminishing when the 1 vol.% ceramic filler were built into the structure of the composite (confirmed by the  $\mu$ CT scans). Pitting was observed on the surface, which

is generally the most common corrosion mechanism for Mg in chloride containing solutions. In this case, with the increasing volume concentration of ceramic filler (5% and 10% by vol.), rapid increase of corrosion rate was observed. This is the result of the significant microgalvanic corrosion which was the predominant corrosion mechanism. This topic was described by our research group in the previous papers describing microgalvanic corrosion [92,102,103], where Dobkowska *et al.* proved that microgalvanic corrosion intensity depends on the number and distribution of cathodes and anodes in the corrosion system. The larger cathodic area, the more intense dissolution of anodic areas, and this is the results of the half-reactions taking place in the corrosive system. When compared two scenarios: with small and large cathodic area, the large cathodic area forces anodic reactions to compensate the local electric neutrality, thus, the intensity of dissolution reactions must increase. In the case of Mg-*Didymosphenia geminata* composites, ceramic filler will serve as cathode when compared to anodic Mg matrix [104,105]. In this scenario, the micro-galvanic corrosion directly corresponds to the area ratio of cathodic to anodic sites of corrosion. In a heterogeneous corrosive system, where the corrosion reactions are strongly dependent on the spatial distribution of the potential of the surface, the larger area of cathodic ceramic filler compared to Mg matrix, increases the dissolution of the alloy.

The results of contact angle measurements show the hydrophilic character of the investigated materials. While the addition of the diatom frustules slightly increased the numerical values of the contact angle, it is still not a proper way to obtain super-hydrophobicity of surface and to significantly lower surface energy of the composites. The manufacturing of the Mg-*Didymosphenia geminata* composites will not lead to a super hydrophobic property of the Mg surface and cannot be a promising technology for improving anticorrosion performance of pure Mg. Finally, among various methods including hydrothermal technique, chemical and electrochemical deposition, the addition of ceramic filler will not replace the strategies used so far – coatings on the surface of alloys [106,107]. Perhaps treatment in the solutions containing modifying agents, including fatty acids or long-chain molecules, should be investigated.

Corrosion resistance of the investigated Mg-based materials was reflected in the cytotoxicity thereof. The most stable composite, *i.e.*, Mg + 1%, was the least cytotoxic, and the least stable, *i.e.*, pure Mg and Mg + 10% *Didymosphenia geminata*, were the most cytotoxic. This observation shows that introduction of small volume fraction of diatoms' frustules reduced the cytotoxicity of pure Mg. The observed cytotoxicity could be attributed to the release of Mg<sup>2+</sup> ions, which increase the pH of medium above physiological values, and change the osmolality thereof [108]. The corrosion of the investigated composites depended also on the type of medium used, and seemed to be faster in  $\alpha$ MEM. In study by Bobe *et al.* [108], the authors suggested that amino acids present in medium could have corrosion-accelerating effect due to formation of complexes with Mg<sup>2+</sup> ions. This is not in com-

pliance with our observations, since the  $\alpha$ MEM contained approximately 20% (molar concentration) and 30% (mass concentration) less of amino acids than DMEM. On the other hand,  $\alpha$ MEM contained  $\sim 1.7$  less sodium bicarbonate, therefore, had lower capacity to buffer the alkaline degradation products than the DMEM. The positive effect of bicarbonate on corrosion resistance of ZM21 in the initial stages of immersion was demonstrated by Witecka *et al.* [109]. It should be noted here that in this study, we incubated the samples in medium w/o FBS in order to prevent adsorption of the FBS molecules on the materials, and, therefore, keep the composition of the FBS constant for all tested materials. This could in turn increase the corrosion of the tested alloys, since FBS was found to maintain the pH of the medium; moreover, the proteins present in the FBS adsorbed on the surface of the samples and formed additional barrier, which lowered the degradation rate [109].

The addition of *Didymosphenia geminata* frustules cause changes in a mean apparent value of coefficient of thermal expansion. In comparison to the CTE for pure Mg, as expected, the addition of siliceous reinforcement resulted in a linear decrease of its value. This restricted elongation during temperature rise may stem from the strong bonding between the metallic matrix and the ceramic particles [110]. It is worth to underline that CTE measured in our work for pure Mg ( $29.3 \pm 0.5 \text{ K}^{-1} \times 10^{-6}$ ) is close to the pure Mg produced by microwave-assisted rapid sintering ( $29.1 \pm 1.2 \text{ K}^{-1} \times 10^{-6}$ ) [111] and to pure Mg manufactured via disintegrated melt deposition technique followed by hot extrusion ( $28.0 \text{ K}^{-1} \times 10^{-6}$ ) [112]. Other study shows that Mg-based composite containing 1% nm-SiC exhibited CTE value of  $28.1 \pm 0.9 \text{ K}^{-1} \times 10^{-6}$ , whereas for 10% of  $\mu\text{m-SiC}$  addition  $25.6 \pm 1.9 \text{ K}^{-1} \times 10^{-6}$  [113]. The latter is close to that obtained in this work for a 10 vol.% *Didymosphenia geminata* frustules.

The thermal conductivity of the samples decreased due to *Didymosphenia geminata* frustules addition. According to our measurements, the sintered composites were characterized by a very high density, supported also by  $\mu\text{CT}$  studies. On that basis, the porosity was determined, which even for the highest value of *Didymosphenia geminata* addition reached only 0.134%. In this regard, neither porosity nor specific heat capacity  $C_p$  (which was assumed the same for all composites) could be the reason of considerable alterations in thermal conductivity values (especially for 5 and 10 vol.% ceramic additive), which according to the results were significantly lower over the entire temperature range than for pure Mg. For the latter, this decrease at room temperature reached almost 56%. This would explain that the main reason for the reduction in thermal conductivity of the composites, as the additive content increased, was the reduction in thermal diffusivity. That could be possibly caused by the increasing content of oxide phases: MgO, SiO<sub>2</sub>, as well as Mg<sub>2</sub>Si (which generally exhibit lower thermal diffusivity values than pure Mg), the presence of which was confirmed by the XRD analysis.

As expected, the addition of *Didymosphenia geminata* frustules improves the mechanical properties of the composites.

The compressive strength and the compressive yield strength of the materials raised with the increasing concentration of *Didymosphenia geminata* frustules. This phenomenon is strongly related to the architecture of the *Didymosphenia geminata* frustules (ribs) which are able to compensate for strain introduced during compression. The finite elements analysis shows that the nature inspired structure of the reinforcement have wide possibilities of applications as the reinforcement in various metal-based matrix [114]. The mechanical potential of the frustules themselves was previously analyzed by Hamm *et al.* [115] and Subhash *et al.* [116]. Both studies focused on the mechanical properties of the frustules determining their mechanical properties in detail. In our previous work, we calculated Young's modulus of the *Didymosphenia geminata* frustules which was found to be 31.8 GPa, and the theoretical consideration about the using the investigated frustules in the complex structures have been considered [117]. The addition of *Didymosphenia geminata* increased microhardness of the materials, and the rise is comparable to the effect which is caused by SiC added to Mg [118,119]. The present research is the first step forward showing the real-life applications of *Didymosphenia geminata* frustules as reinforcement in Mg-based composites with higher mechanical properties than those of pure Mg.

Mg-based composites with *Didymosphenia geminata* frustules represent a promising material with properties showing excellent prospects for producing bulk materials with applications in various fields. We proved that trace addition of *Didymosphenia geminata* frustules into the Mg matrix may improve its corrosion resistance and mechanical properties which, considering bioapplications, is of critical importance. The results of this work clearly show that the formation of Mg<sub>2</sub>Si increases corrosion performance of the Mg – *Didymosphenia geminata* composites since Mg<sub>2</sub>Si is cathodic with respect to the Mg matrix. Moreover, MgO easily transforms to Mg(OH)<sub>2</sub> by hydration, and it further decomposes to Mg<sup>2+</sup> [42]. Taking this into consideration the formation of Mg<sub>2</sub>Si and MgO mixtures may lead to the full degradation of the material, which is obviously important considering biodegradable materials, however, the issue of cytotoxicity due to increasing content of the ceramic filler should be further investigated. Simultaneously, presence of Mg<sub>2</sub>Si [120] and MgO [43] plays a significant role in the mechanical properties by strengthening of the material in terms of increase in compressive strength, compressive yield strength and microhardness improvement, which is crucial for load bearing applications.

## 6. Conclusions

In this work, a new generation of Mg-based composites with natural filler were produced and investigated. Based on the results the following conclusions can be drawn:

1. Mg + *Didymosphenia geminata* composites produced using pulse plasma sintering (PPS) are characterized by uniform distribution of the ceramic filler in metallic matrix regardless of content of the filler (1, 5 or 10 vol.%).

- Porosity of the samples is generally low, 0.006% for pure Mg. It increases with addition of frustules from 0.004 for Mg + 1 vol.%, 0.025 for Mg + 5 vol.% to 0.134% for Mg + 10 vol.% *Didymosphenia geminata* frustules.
- The addition of 1 vol.% *Didymosphenia geminata* frustules has a positive impact on the corrosion and biological response of Mg. The addition of 1 vol.% ceramic filler changes the mechanism of corrosion causing passivation of the surface. The passivation layer is expected to limit hydrogen release of material, which is of crucial importance in clinic use. The non-cytotoxic behavior is still observed for the addition of 5 vol.% *Didymosphenia geminata* frustules, but this content lowers corrosion resistance of the composite. A higher concentration of filler leads to strong microgalvanic corrosion and increase in cytotoxicity.
  - The coefficient of thermal expansion values exhibit a linear decrease as the amount of the *Didymosphenia geminata* frustules increased. The addition of natural ceramic filler causes a reduction in thermal conductivity (significant for 5 and 10 vol.% *Didymosphenia geminata*) over the entire temperature range, which was attributed to hampered thermal diffusivity.
  - With the increased addition of *Didymosphenia geminata* frustules, an increase in strength with a decrease in compressive strain is observed. Even the smallest addition of *Didymosphenia geminata* frustules to the Mg matrix causes a significant increase in microhardness; 1 vol.% *Didymosphenia geminata* caused an increase in microhardness about 23%, 5 vol.% about 52% whereas the highest amount of ceramic filler results in the microhardness improvement of about 102%.
  - The natural filler in the form of *Didymosphenia geminata* frustules may significantly change properties of pure Mg, indicating wide potential for biomedical applications of Mg-based implants.

### CRedit authorship contribution statement

IBZ: Conceptualization, Methodology, Investigation, Formal analysis, Data curation, Visualization, Writing – original draft preparation, Writing – review & editing, Supervision, Funding acquisition, Resources. AD: Conceptualization, Methodology, Investigation, Formal analysis, Data curation, Visualization, Writing – original draft preparation, Writing – review & editing. AZ: Investigations and Formal Analysis, Visualization. EB: Investigations and Formal Analysis, Visualization. MJK: Investigations, Formal Analysis (sample manufacturing), Visualization, Writing – review & editing. RZ: Investigations, Visualization, Writing – review & editing. TP: Investigations, Visualization, Writing – review & editing. JI: Investigations, Visualization, Writing – original draft preparation. JJ: Investigations, Visualization, Writing – review & editing. KP: Investigations, Visualization, Writing – review & editing. BAC: Investigation. KN: Investigations, Visualization, Writing – review & editing. BB: Investigations, Visualization, Writing – review & editing. WS: Supervision,

Resources, Writing – review & editing. KJK: Supervision, Resources, Writing – review & editing.

### Data availability statement

The raw/processed data required to reproduce these findings are available from the corresponding authors: [i.zglobicka@pb.edu.pl](mailto:i.zglobicka@pb.edu.pl) (IBZ) or [anna.dobkowska@pw.edu.pl](mailto:anna.dobkowska@pw.edu.pl) (AD) on request.

### Declaration of competing interest

The authors declare that they have no known competing financial interests or personal relationships that could have appeared to influence the work reported in this paper.

### Acknowledgement

Izabela B. Zgłobicka acknowledges the funding provided by National Science Center for providing financial support to project Metal Matrix Composites with natural filler (Grant No. 2018/31/D/ST8/00890). The authors are grateful to Dr Matt P. Ashworth from the University of Texas at Austin (USA) for critically reading the manuscript and correcting the language.

### References

- [1] R. Verma, J.T. Carter, Quick Plastic Forming of a Decklid Inner Panel with Commercial AZ31 Magnesium Sheet, 2006, doi:[10.4271/2006-01-0525](https://doi.org/10.4271/2006-01-0525).
- [2] S. Logan, A. Kizyma, C. Patterson, S. Rama, Lightweight Magnesium Intensive Body Structure, 2006, doi:[10.4271/2006-01-0523](https://doi.org/10.4271/2006-01-0523).
- [3] A.A. Luo, J. Magnes. Alloy. 1 (2013) 2–22, doi:[10.1016/j.jma.2013.02.002](https://doi.org/10.1016/j.jma.2013.02.002).
- [4] R. Radha, D. Sreekanth, J. Magnes. Alloy. 5 (2017) 286–312, doi:[10.1016/j.jma.2017.08.003](https://doi.org/10.1016/j.jma.2017.08.003).
- [5] A. Abbas, V. Rajagopal, S.-J. Huang, Magnes. Alloy. Struct. Prop. (2022) IntechOpen, doi:[10.5772/intechopen.96241](https://doi.org/10.5772/intechopen.96241).
- [6] M.K. Kulekci, Int. J. Adv. Manuf. Technol. 39 (2008) 851–865, doi:[10.1007/s00170-007-1279-2](https://doi.org/10.1007/s00170-007-1279-2).
- [7] L.A. Dobrzański, G.E. Totten, M. Bamberger (Eds.), Magnesium and Its Alloys, CRC Press, Boca Raton, FL, 2019 First editionCRC Press/Taylor & Francis Group, [2020] Series: Metals and alloys, doi:[10.1201/9781351045476](https://doi.org/10.1201/9781351045476).
- [8] J. Zhang, R.J. Perez, E.J. Lavernia, J. Mater. Sci. 28 (1993) 2395–2404, doi:[10.1007/BF01151671](https://doi.org/10.1007/BF01151671).
- [9] S. Lee, H.J. Ham, S.Y. Kwon, S.W. Kim, C.M. Suh, Int. J. Thermophys. 34 (2013) 2343–2350, doi:[10.1007/s10765-011-1145-1](https://doi.org/10.1007/s10765-011-1145-1).
- [10] S. Li, X. Yang, J. Hou, W. Du, J. Magnes. Alloy. 8 (2020) 78–90, doi:[10.1016/j.jma.2019.08.002](https://doi.org/10.1016/j.jma.2019.08.002).
- [11] V.K. Bommala, M.G. Krishna, C.T. Rao, J. Magnes. Alloy. 7 (2019) 72–79, doi:[10.1016/j.jma.2018.11.001](https://doi.org/10.1016/j.jma.2018.11.001).
- [12] G.L. Song, A. Atrens, Adv. Eng. Mater. 1 (1999) 11–33, doi:[10.1002/\(SICI\)1527-2648\(199909\)1:1\(11::AID-ADEM11\)3.0.CO;2-N](https://doi.org/10.1002/(SICI)1527-2648(199909)1:1(11::AID-ADEM11)3.0.CO;2-N).
- [13] F. Witte, J. Fischer, J. Nellesen, C. Vogt, J. Vogt, T. Donath, F. Beckmann, Acta Biomater. 6 (2010) 1792–1799, doi:[10.1016/j.actbio.2009.10.012](https://doi.org/10.1016/j.actbio.2009.10.012).
- [14] K. kun Deng, X. jun Wang, C. ju Wang, J. yan Shi, X. shi Hu, K. Wu, Mater. Sci. Eng. A 553 (2012) 74–79, doi:[10.1016/j.msea.2012.05.094](https://doi.org/10.1016/j.msea.2012.05.094).
- [15] K.B. Nie, X.J. Wang, K.K. Deng, X.S. Hu, K. Wu, J. Magnes. Alloy. 9 (2021) 57–77, doi:[10.1016/j.jma.2020.08.018](https://doi.org/10.1016/j.jma.2020.08.018).

- [16] F. Khorashadizade, S. Abazari, M. Rajabi, H.R. Bakhsheshi-Rad, A.F. Ismail, S. Sharif, S. Ramakrishna, F. Berto, J. Mater. Res. Technol. 15 (2021) 6034–6066, doi:10.1016/j.jmrt.2021.10.141.
- [17] S.M. Khaled, R. Sui, P.A. Charpentier, A.S. Rizkalla, Langmuir 23 (2007) 3988–3995, doi:10.1021/la062879n.
- [18] H. Khoshzaban Khosroshahi, F. Fereshteh Saniee, H.R. Abedi, Mater. Sci. Eng. A 595 (2014) 284–290, doi:10.1016/j.msea.2013.12.029.
- [19] G.K. Meenashisundaram, M.H. Nai, A. Almajid, M. Gupta, Mater. Des. 65 (2015) 104–114, doi:10.1016/j.matdes.2014.08.041.
- [20] S.F. Hassan, M.J. Tan, M. Gupta, Mater. Sci. Technol. 23 (2007) 1309–1312, doi:10.1179/174328407X236913.
- [21] S.F. Hassan, M. Gupta, J. Mater. Sci. 41 (2006) 2229–2236, doi:10.1007/s10853-006-7178-3.
- [22] M. Navazani, K. Dehghani, J. Mater. Process. Technol. 229 (2016) 439–449, doi:10.1016/j.jmatprotec.2015.09.047.
- [23] S.F. Hassan, M. Gupta, J. Compos. Mater. 41 (2007) 2533–2543, doi:10.1177/0021998307074187.
- [24] R. Vaira Vignesh, R. Padmanaban, M. Govindaraju, G. Suganya Priyadharshini, Trans. IMF 97 (2019) 261–270, doi:10.1080/00202967.2019.1648005.
- [25] K. Rahmani, G.H. Majzoobi, A. Sadooghi, M. Kashfi, Mater. Chem. Phys. 246 (2020) 122844, doi:10.1016/j.matchemphys.2020.122844.
- [26] A.K. Khanra, H.W.A.C. Jung, S.H. Yu, K.U.G.S. Hong, in: *Microstructure and Mechanical Properties of Mg – HAP Composites*, 33, 2010, pp. 43–47.
- [27] A. Feng, Y. Han, Mater. Des. 32 (2011) 2813–2820, doi:10.1016/j.matdes.2010.12.054.
- [28] R. del Campo, B. Savoini, A. Muñoz, M.A. Monge, G. Garcés, J. Mech. Behav. Biomed. Mater. 39 (2014) 238–246, doi:10.1016/j.jmbbm.2014.07.014.
- [29] S. Dutta, S. Gupta, M. Roy, ACS Biomater. Sci. Eng. 6 (2020) 4748–4773, doi:10.1021/acsbomaterials.0c00678.
- [30] Z. Cui, Y. Zhang, Y. Cheng, D. Gong, W. Wang, Mater. Sci. Eng. C 99 (2019) 1035–1047, doi:10.1016/j.msec.2019.02.050.
- [31] S.-H. Kwon, Y.-K. Jun, S.-H. Hong, H.-E. Kim, J. Eur. Ceram. Soc. 23 (2003) 1039–1045, doi:10.1016/S0955-2219(02)00263-7.
- [32] M. Razavi, M.H. Fathi, M. Meratian, Mater. Charact. 61 (2010) 1363–1370, doi:10.1016/j.matchar.2010.09.008.
- [33] Y. Yang, C. Lu, L. Shen, Z. Zhao, S. Peng, C. Shuai, J. Magnes. Alloy. (2021), doi:10.1016/j.jma.2021.04.009.
- [34] Y. Yin, Q. Huang, L. Liang, X. Hu, T. Liu, Y. Weng, T. Long, Y. Liu, Q. Li, S. Zhou, H. Wu, J. Alloys Compd. 785 (2019) 38–45, doi:10.1016/j.jallcom.2019.01.165.
- [35] J.R. Jones, Acta Biomater. 9 (2013) 4457–4486, doi:10.1016/j.actbio.2012.08.023.
- [36] K. Kuśnierczyk, M. Basista, J. Biomater. Appl. 31 (2017) 878–900, doi:10.1177/0885328216657271.
- [37] A.A. El-Rashidy, J.A. Roether, L. Harhaus, U. Kneser, A.R. Boccacini, Acta Biomater. 62 (2017) 1–28, doi:10.1016/j.actbio.2017.08.030.
- [38] S. Dutta, K.B. Devi, S. Gupta, B. Kundu, V.K. Balla, M. Roy, J. Biomed. Mater. Res. Part B Appl. Biomater. 107 (2019) 352–365, doi:10.1002/jbm.b.34127.
- [39] L.L. Hench, Biomed. Glas. 1 (2015) 1–11, doi:10.1515/bglass-2015-0001.
- [40] C. Wu, J. Chang, J. Wang, S. Ni, W. Zhai, Biomaterials 26 (2005) 2925–2931, doi:10.1016/j.biomaterials.2004.09.019.
- [41] S.N. Dezfouli, Z. Huan, A. Mol, S. Leeftang, J. Chang, J. Zhou, Mater. Sci. Eng. C 79 (2017) 647–660, doi:10.1016/j.msec.2017.05.021.
- [42] T. Lei, W. Tang, S.-H. Cai, F.-F. Feng, N.-F. Li, Corros. Sci. 54 (2012) 270–277, doi:10.1016/j.corsci.2011.09.027.
- [43] C.S. Goh, M. Gupta, J. Wei, L.C. Lee, J. Compos. Mater. 41 (2007) 2325–2335, doi:10.1177/0021998307075445.
- [44] G. Lin, D. Liu, M. Chen, C. You, Z. Li, Y. Wang, W. Li, Mater. Charact. 144 (2018) 120–130, doi:10.1016/j.matchar.2018.06.028.
- [45] C. Shuai, B. Wang, S. Bin, S. Peng, C. Gao, Mater. Des. 191 (2020) 108612, doi:10.1016/j.matdes.2020.108612.
- [46] I. Nakahata, Y. Tsutsumi, E. Kobayashi, Metals 10 (2020) 1–14.
- [47] S. Dutta, K.B. Devi, S. Mandal, A. Mahato, S. Gupta, B. Kundu, V.K. Balla, M. Roy, Materialia 5 (2019) 100245, doi:10.1016/j.mtl.2019.100245.
- [48] F. Delannay, Compr. Compos. Mater. (2000) 341–369 Elsevier, doi:10.1016/B0-08-042993-9/00013-9.
- [49] P. Lukac, A. Rudajeva, Kov. Mater. 41 (2003) 281–292.
- [50] S. Elomari, M.D. Skibo, A. Sundarajan, H. Richards, Compos. Sci. Technol. 58 (1998) 369–376, doi:10.1016/S0266-3538(97)00124-3.
- [51] R. Arpón, J.M. Molina, R.A. Saravanan, C. García-Cordovilla, E. Louis, J. Narciso, Acta Mater. 51 (2003) 3145–3156, doi:10.1016/S1359-6454(03)00126-5.
- [52] N. Chawla, X. Deng, D.R.M. Schnell, Mater. Sci. Eng. A 426 (2006) 314–322, doi:10.1016/j.msea.2006.04.054.
- [53] Y.-L. Shen, A. Needleman, S. Suresh, Metall. Mater. Trans. A 25 (1994) 839–850, doi:10.1007/BF02665460.
- [54] T. Wejrzanowski, M. Grybczuk, M. Chmielewski, K. Pietrzak, K.J. Kurzydłowski, A. Strojny-Nedza, Mater. Des. 99 (2016) 163–173, doi:10.1016/j.matdes.2016.03.069.
- [55] Ł. Ciupiński, M.J. Kruzewski, J. Grzonka, M. Chmielewski, R. Zieliński, D. Moszczyńska, A. Michalski, Mater. Des. 120 (2017) 170–185, doi:10.1016/j.matdes.2017.02.005.
- [56] L.C. Davis, B.E. Artz, J. Appl. Phys. 77 (1995) 4954–4960, doi:10.1063/1.359302.
- [57] A.Lo Conte, Metal Matrix Composites: Design Methodology, Wiley Encycl. Compos., John Wiley & Sons, Inc., Hoboken, NJ, USA, 2012, doi:10.1002/9781118097298.weoc141.
- [58] I. Zgłobicka, J. Gluch, Z. Liao, S. Werner, P. Guttman, Q. Li, P. Bazarnik, T. Plocinski, A. Witkowski, K.J. Kurzydłowski, Sci. Rep. 11 (2021) 14555, doi:10.1038/s41598-021-94069-9.
- [59] P.J. Lopez, J. Desclés, A.E. Allen, C. Bowler, Curr. Opin. Biotechnol. 16 (2005) 180–186, doi:10.1016/j.copbio.2005.02.002.
- [60] R. Gordon, D. Losic, M.A. Tiffany, S.S. Nagy, F.A.S. Sterrenburg, Trends Biotechnol. 27 (2009) 116–127, doi:10.1016/j.tibtech.2008.11.003.
- [61] M. Dobrosielska, R. Przekop, B. Sztorch, D. Brząkałski, I. Zgłobicka, M. Łepicka, R. Dobosz, K. Kurzydłowski, Materials 13 (2020) 4632, doi:10.3390/ma13204632.
- [62] M. Dobrosielska, R. Dobrucka, D. Brząkałski, M. Gloc, J. Rębiś, J. Głowacka, K.J. Kurzydłowski, R.E. Przekop, Materials 14 (2021) 4607, doi:10.3390/ma14164607.
- [63] M. Dobrosielska, R. Dobrucka, D. Brząkałski, M. Frydrych, P. Kozera, M. Wiczorek, M. Jałbrzykowski, K.J. Kurzydłowski, R.E. Przekop, Materials 15 (2022) 3607, doi:10.3390/ma15103607.
- [64] I. Zgłobicka, R. Zybala, K. Kaszyca, R. Molak, M. Wiczorek, K. Recko, B. Fiedoruk, K.J. Kurzydłowski, Sci. Rep. 12 (2022) 1–10, doi:10.1038/s41598-022-12855-5.
- [65] I. Zgłobicka, M. Joka Yildiz, R. Molak, M. Kawalec, A. Dubicki, J. Wroblewski, K. Dydek, A. Boczkowska, K.J. Kurzydłowski, Materials 15 (2022) 1–11.
- [66] S. Ramakrishna, J. Mayer, E. Wintermantel, K.W. Leong, Compos. Sci. Technol. 61 (2001) 1189–1224, doi:10.1016/S0266-3538(00)00241-4.
- [67] G. Xiong, Y. Nie, D. Ji, J. Li, C. Li, W. Li, Y. Zhu, H. Luo, Y. Wan, Curr. Appl. Phys. 16 (2016) 830–836, doi:10.1016/j.cap.2016.05.004.
- [68] H. Zheng, Z. Li, M. Chen, C. You, D. Liu, Mater. Sci. Eng. A 715 (2018) 205–213, doi:10.1016/j.msea.2018.01.006.
- [69] M. Shahin, K. Munir, C. Wen, Y. Li, Acta Biomater. 96 (2019) 1–19, doi:10.1016/j.actbio.2019.06.007.
- [70] X. Li, G. Ma, P. Jin, L. Zhao, J. Wang, S. Li, J. Alloys Compd. 778 (2019) 309–317, doi:10.1016/j.jallcom.2018.11.110.
- [71] K.S. Tun, M. Gupta, Compos. Sci. Technol. 67 (2007) 2657–2664, doi:10.1016/j.compscitech.2007.03.006.
- [72] E. Ghasali, A. Bordbar-Khiabani, M. Alizadeh, M. Mozafari, M. Niazmand, H. Kazemzadeh, T. Ebadzadeh, Mater. Chem. Phys. 225 (2019) 331–339, doi:10.1016/j.matchemphys.2019.01.007.
- [73] X. Wang, P. Zhang, L.H. Dong, X.L. Ma, J.T. Li, Y.F. Zheng, Mater. Des. 54 (2014) 995–1001, doi:10.1016/j.matdes.2013.09.037.

- [74] Y. Yang, C. He, E. Dianyu, W. Yang, F. Qi, D. Xie, L. Shen, S. Peng, C. Shuai, *Mater. Des.* 185 (2020) 108259, doi:10.1016/j.matdes.2019.108259.
- [75] A.K. Khanra, H.C. Jung, S.H. Yu, K.S. Hong, K.S. Shin, *Bull. Mater. Sci.* 33 (2010) 43–47, doi:10.1007/s12034-010-0006-z.
- [76] K. Wu, K. Deng, K. Nie, Y. Wu, X. Wang, X. Hu, M. Zheng, *Mater. Des.* 31 (2010) 3929–3932, doi:10.1016/j.matdes.2010.03.021.
- [77] F. Cao, Z. Shi, G.-L. Song, M. Liu, M.S. Dargusch, A. Atrens, *Corros. Sci.* 90 (2015) 176–191, doi:10.1016/j.corsci.2014.10.012.
- [78] C.C. Ng, M.M. Savalani, H.C. Man, I. Gibson, *Virtual Phys. Prototyp.* 5 (2010) 13–19, doi:10.1080/17452751003718629.
- [79] Y. Li, J. Zhou, P. Pavanram, M.A. Leeftang, L.I. Fockaert, B. Poursan, N. Tümer, K.-U. Schröder, J.M.C. Mol, H. Weinans, H. Jahr, A.A. Zadpoor, *Acta Biomater.* 67 (2018) 378–392, doi:10.1016/j.actbio.2017.12.008.
- [80] R. Xu, M.-C. Zhao, Y.-C. Zhao, L. Liu, C. Liu, C. Gao, C. Shuai, A. Atrens, *Mater. Lett.* 237 (2019) 253–257, doi:10.1016/j.matlet.2018.11.071.
- [81] R. Karunakaran, S. Orgies, A. Tamayol, F. Bobaru, M.P. Sealy, *Bioact. Mater.* 5 (2020) 44–54, doi:10.1016/j.bioactmat.2019.12.004.
- [82] Y. Yang, C. Lu, S. Peng, L. Shen, D. Wang, F. Qi, C. Shuai, *Virtual Phys. Prototyp.* 15 (2020) 278–293, doi:10.1080/17452759.2020.1748381.
- [83] D. Annur, A. Suhardi, M.I. Amal, M.S. Anwar, I. Kartika, J. Phys. Conf. Ser. 817 (2017) 012062, doi:10.1088/1742-6596/817/1/012062.
- [84] B.R. Sunil, R. Dumpala, *Encycl. Mater. Compos.* (2021) 770–780 Elsevier Ltd., doi:10.1016/b978-0-12-803581-8.11917-4.
- [85] I. Zgłobicka, *Int. J. Algae* 15 (2013) 291–310, doi:10.1615/InterJAlgae.v15.i4.10.
- [86] I. Zgłobicka, Q. Li, J. Gluch, M. Płocińska, T. Noga, R. Dobosz, R. Szoszkiewicz, A. Witkowski, E. Zschech, K.J. Kurzydłowski, *Sci. Rep.* 7 (2017) 1–7, doi:10.1038/s41598-017-08960-5.
- [87] M.J. Kruszewski, R. Zybala, Ł. Ciupiński, M. Chmielewski, B. Adamczyk-Cieślak, A. Michalski, M. Rajaska, K.J. Kurzydłowski, *J. Electron. Mater.* 45 (2016) 1369–1376, doi:10.1007/s11664-015-4037-5.
- [88] D. Pałgan, A. Dobkowska, A. Zielińska, D. Drozdenko, K. Máthiś, W. Świąszkowski, *Crystals* 12 (2022) 1723, doi:10.3390/cryst12121723.
- [89] A. Dobkowska, M. Koralnik, B. Adamczyk-Cieślak, D. Kuc, W. Chromiński, J. Kubasek, J. Mizera, *J. Mater. Eng. Perform.* 31 (2022) 8932–8939, doi:10.1007/s11665-022-06895-1.
- [90] A. Dobkowska, Ł. Żrodowski, M. Chlewicka, M. Koralnik, B. Adamczyk-Cieślak, J. Ciftci, B. Morończyk, M. Kruszewski, J. Jaroszewicz, D. Kuc, W. Świąszkowski, J. Mizera, J. Magnes. Alloy. 10 (2022) 3553–3564, doi:10.1016/j.jma.2022.06.003.
- [91] ISO 10993-5: *Biological Evaluation of Medical Devices*, 2009.
- [92] A. Dobkowska, B. Adamczyk – Cieślak, M. Koralnik, W. Chromiński, J. Kubasek, J. Ciftci, D. Kuc, J. Mizera, J. Magnes. Alloy. 10 (2022) 811–820, doi:10.1016/j.jma.2021.08.020.
- [93] C.Q. Li, D.K. Xu, X.-B. Chen, B.J. Wang, R.Z. Wu, E.H. Han, N. Birbilis, *Electrochim. Acta.* 260 (2018) 55–64, doi:10.1016/j.electacta.2017.11.091.
- [94] A.D. King, N. Birbilis, J.R. Scully, *Electrochim. Acta.* 121 (2014) 394–406, doi:10.1016/j.electacta.2013.12.124.
- [95] H. Li, S. Pang, Y. Liu, L. Sun, P.K. Liaw, T. Zhang, *Mater. Des.* 67 (2015) 9–19, doi:10.1016/j.matdes.2014.10.085.
- [96] X. Fu, R. Deng, X. Kong, G. Parande, J. Hu, P. Peng, Z. Zhu, B. Shi, G. Wang, M. Gupta, R.O. Ritchie, *Acta Mater.* 230 (2022) 117840, doi:10.1016/j.actamat.2022.117840.
- [97] I. Gutman, L. Klinger, I. Gotman, M. Shapiro, *Scr. Mater.* 45 (2001) 363–367, doi:10.1016/S1359-6462(01)01043-0.
- [98] I. Gutman, I. Gotman, M. Shapiro, *Acta Mater.* 54 (2006) 4677–4684, doi:10.1016/j.actamat.2006.05.048.
- [99] M. Aydin, F. Findik, *Ind. Lubr. Tribol.* 62 (2010) 232–237, doi:10.1108/00368791011051099.
- [100] S. Tiwari, R. Balasubramaniam, M. Gupta, *Corros. Sci.* 49 (2007) 711–725, doi:10.1016/j.corsci.2006.05.047.
- [101] N.N. Aung, W. Zhou, C.S. Goh, S.M.L. Nai, J. Wei, *Corros. Sci.* 52 (2010) 1551–1553, doi:10.1016/j.corsci.2010.02.025.
- [102] A. Dobkowska, B. Adamczyk – Cieślak, J. Kubasek, D. Vojtěch, D. Kuc, E. Hadasik, J. Mizera, J. Magnes. Alloy. 9 (2021) 467–477, doi:10.1016/j.jma.2020.07.007.
- [103] A. Dobkowska, M.D.H. Castillo, J.P. Turnbull, S. Ramamurthy, D. Zavidulin, D.E. Moser, M. Behazin, P.G. Keech, D.W. Shoesmith, J.J. Noël, *Corros. Sci.* 192 (2021) 109778, doi:10.1016/j.corsci.2021.109778.
- [104] G. Ben-Hamu, D. Eliezer, K.S. Shin, *Mater. Sci. Eng. A* 447 (2007) 35–43, doi:10.1016/j.msea.2006.10.059.
- [105] A.D. Südholz, N.T. Kirkland, R.G. Buchheit, N. Birbilis, *Electrochim. Solid-State Lett.* 14 (2011) C5, doi:10.1149/1.3523229.
- [106] B. Yin, L. Fang, J. Hu, A.-Q. Tang, W.-H. Wei, J. He, *Appl. Surf. Sci.* 257 (2010) 1666–1671, doi:10.1016/j.apsusc.2010.08.119.
- [107] M. Yeganeh, N. Mohammadi, *J. Magnes. Alloy.* 6 (2018) 59–70, doi:10.1016/j.jma.2018.02.001.
- [108] K. Bobe, E. Willbold, I. Morgenthal, O. Andersen, T. Studnitzky, J. Nellesen, W. Tillmann, C. Vogt, K. Vano, F. Witte, *Acta Biomater.* 9 (2013) 8611–8623, doi:10.1016/j.actbio.2013.03.035.
- [109] A. Witecka, A. Bogucka, A. Yamamoto, K. Máthiś, T. Krajňák, J. Jaroszewicz, W. Świąszkowski, *Mater. Sci. Eng. C* 65 (2016) 59–69, doi:10.1016/j.msec.2016.04.019.
- [110] M.N. Arif, M.Z. Bukhari, D. Brabazon, M.S.J. Hashmi, *IOP Conf. Ser. Mater. Sci. Eng.* 701 (2019) 012057, doi:10.1088/1757-899X/701/1/012057.
- [111] W.L.E. Wong, M. Gupta, *Materials* (2005) 453–459, ASMECD, doi:10.1115/IMECE2005-82502.
- [112] S. Ugandhar, M. Gupta, S.K. Sinha, *Solid State Phenom.* 111 (2006) 79–82, doi:10.4028/www.scientific.net/SSP.111.79.
- [113] W.L.E. Wong, M. Gupta, *Solid State Phenom.* 111 (2006) 91–94, doi:10.4028/www.scientific.net/SSP.111.91.
- [114] A. Dubicki, I. Zgłobicka, K.J. Kurzydłowski, *Metals* 11 (2021) 881, doi:10.3390/met11060881.
- [115] C.E. Hamm, R. Merkel, O. Springer, P. Jurkojc, C. Maiert, K. Prechtelt, V. Smetacek, *Nature* 421 (2003) 841–843, doi:10.1038/nature01416.
- [116] G. Subhash, S. Yao, B. Bellinger, M.R. Gretz, *J. Nanosci. Nanotechnol.* 5 (2005) 50–56, doi:10.1166/jnn.2005.006.
- [117] E. Topal, H. Rajendran, I. Zgłobicka, J. Gluch, Z. Liao, A. Clausner, K. Kurzydłowski, E. Zschech, *Nanomaterials* 10 (2020) 959, doi:10.3390/nano10050959.
- [118] D. Penher, A. Ghasemi, R. Riedel, C. Fleck, S. Kamrani, *Mater. Sci. Eng. A* 738 (2018) 264–272, doi:10.1016/j.msea.2018.09.106.
- [119] K. Rahmani, G. Majzoobi, A. Atrian, *J. Compos. Mater.* 54 (2020) 659–668, doi:10.1177/0021998319864629.
- [120] W. Jiang, X. Xu, Y. Zhao, Z. Wang, C. Wu, D. Pan, Z. Meng, *Mater. Sci. Eng. A* 721 (2018) 263–273, doi:10.1016/j.msea.2018.02.100.